Available online at www.sciencedirect.com

ScienceDirect

Journal of Magnesium and Alloys xxx (xxxx) xxx

www.elsevier.com/locate/jma

Review

Review on the effect of different processing techniques on the microstructure and mechanical behaviour of AZ31 Magnesium alloy

Rakshith M., Seenuvasaperumal P.*

School of Mechanical Engineering, Vellore Institute of Technology, Vellore, 632014, India

Received 4 November 2020; received in revised form 8 February 2021; accepted 24 March 2021
Available online xxx

Abstract

Magnesium (Mg) alloys despite being the ideal candidate for structural applications, owing to their high specific strength and low density, are not widely used due to lack of active slip systems at room temperature in their hexagonal close-packed crystal structure, eliciting poor ductility and formability. Amongst the various series of Mg alloys, the AZ and ZK series alloys have been standouts, as they inherit better room temperature strength and flow characteristics through their solute elements. Grain refinement, as well as eliminating casting defects through metal processing techniques are vital for the commercial viability of these alloys since they play a key role in controlling the mechanical behaviour. As such, this review highlights the effect of different Bulk-deformation and Severe Plastic Deformation techniques on the crystal orientation and the corresponding mechanical behaviours of the AZ31 alloy. However, every process parameter surrounding these techniques must be well thought of, as they require specially designed tools. With the advent of finite element analysis, these processes could be computationally realized for different parameters and optimized in an economically viable manner. Hence, this article also covers the developments made in finite element methods towards these techniques.

Keywords: AZ31 magnesium alloy; Severe plastic deformation process; Rolling; Extrusion; Finite element simulation.

1. Introduction

Vehicles are the inevitable mode of transportation. As time progresses, demand and usage of crude oil have always been increasing. However, fluctuation in crude oil prices and its limited availability is threatening to the automobile and aerospace domain. Also, it is proved that increased usage of these vehicles contributes to the greenhouse effect due to its exhaust emission gas. Thus, reducing fuel usage and the rate of exhaust gas emissions is a challenging task [1,2]. In this regard, engineers and scientists are performing research on alternate fuels and weight reduction methods for vehicle structures. By using lightweight metals, a structure could be optimized for reduced fuel usage.

Mg is believed to be the right alternative for conventional metals (Aluminium, Titanium, iron, etc.) used in automotive and aerospace structural applications, with desirable properties such as low density, high specific strength, easy recyclability, and yet economical. However, limitations such as poor ductility, corrosion, and wear resistance are restricting its usage in real-world applications [3,4]. As per Von-Mises criteria, 5 independent slip systems are required to enable uniform plastic deformation [3,5]. This is unfulfilled for pure Mg, as plastic flow is only realized through basal slip at room temperature. To overcome these limitations, Mg-based alloys are widely found in different series (AZ, AM, AXE, ZE, ZK, etc.) with varieties of soluble elements [1,2]. Amongst these, AZ31 alloy is widely used due to its abundant commercial availability and good tensile characteristics, AZ31 alloy's chemical composition is shown in Table. 1. However, AZ31 alloy usages are limited in as-cast condition due to low yield strength and the casting defects [2].

* Corresponding author.
E-mail address: seenumeed@gmail.com (Rakshith M.).

https://doi.org/10.1016/j.jma.2021.03.019

Table 1
Chemical composition of AZ31 Mg Alloy [2].

AZ31 Mg Alloy							
Designation	Al	Zn	Mn	Cu	Ni	Si	Mg
Mass%	2.5–3.5	0.7–1.3	0.2	0.05	0.005	0.05	Balance

Hall–Petch relation demonstrates that grain refinement is a promising method for improving yield strength [6]. Thus, these alloys are formed with secondary processes like rolling and extrusion processes, which results in enhanced yield strength through refined grains. Also, it was accepted that severe plastic deformation (SPD) processes could also be performed on Mg alloys to achieve grain sizes in the ultra-fine grain (UFG) range or even in the nano range [7]. With this level of grain refinement in AZ31 alloy, grain boundary sliding can be activated at room temperature leading to quasi-superplastic elongations. The current author has experience in this discipline, by performing the High-Pressure Torsion (HPT) process to achieve grain size about nanoscale for AZ31 alloy [4].

Nonetheless, the above-mentioned techniques are controlled by their respective processing parameters, which subsequently influence the grain size morphology and basal plane orientation [4]. Secondary processes such as these are vital for making AZ31 alloys compatible for real-world applications, as long as it is economically feasible. And this is where Finite Element Analysis (FEA) is useful, by simulating the thermo-mechanics behind these techniques. This is essential for cost-effective process optimization [8]. Various secondary processing techniques of AZ31 alloy and the related FEA behind them will be elucidated in this review.

2. Bulk deformation processing techniques

Metal forming operations performed to transform billets of one shape into another is commonly known as Bulk Deformation Processing Techniques. This is accomplished through the use of metal forming tools, where materials are plastically deformed to achieve the desired shape and mechanical properties. There are two major bulk deformation techniques used to process AZ31 alloy: Rolling, and Extrusion. These processes as schematically illustrated in Fig. 1.

2.1. Rolling

Rolling as a metal forming operation is done to produce metals in the form of sheet, bars, sections, and tubes [9]. Here, one or more rolling mills are placed in an arrangement, such that the work piece can be inserted between these mills, as schematically shown in Fig. 1(a). The friction between the rolls and the work piece is the driving force that pushes the material forward, and the loads exerted by the mills compress the work piece to a lower thickness. Thus, the desired mechanical property is achieved through the resulting microstructure refinement. However, this is influenced by processing parameters such as rolling speed, number of passes, thickness reduction ratio, and most importantly, the working temperature. Thus, the rolling process can be classified broadly by the working temperature: hot rolling, cold rolling, and cryogenic rolling. The effect of these respective processing parameters over the material property of AZ31 alloy is discussed broadly in sub-sections.

2.1.1. Hot rolling

Hot rolling process is usually carried out above the recrystallization temperature of a particular metal [9]. Generally, the number of passes, rolling speed, and initial texture are the important microstructure refining parameters in hot rolling. However, the number of passes crucially depends on the desired reduction of thickness. The reduction can be achieved through multiple passes with a small reduction% per pass. But it has proven to be less efficient and expensive for AZ31 alloy, as intermediate annealing is required to maintain the pass-to-pass workability and suppress edge cracks or material fracture [10]. Thus, high thickness reduction and fewer number of passes are preferred for the pronounced effect of dynamic recrystallization (DRX). The effect of variation in reduction% in AZ31 alloy can be observed through the microstructure orientation maps shown in Fig. 2 [11].

Also, DRX behaviour can be controlled by rolling speed [12]. This is because deformation energy in the rolling process is consumed in different ways at different rolling speeds. At low speed, part of deformation energy is absorbed and stored by lattice defects such as twinning. While the rest is released by edge cracking [10,12]. The presence of twinning behaviour promotes strain hardening of the material, and the subsequent grain refinement increases the strength of the AZ31 alloy. However, at higher speeds, the heat energy transferred to rollers is less, which promotes DRX and grain growth. Thus, high-speed rolling is preferred to enhance the stretch formability of the AZ31 alloy at room temperature, as it extends DRX [12,13,15]. Additionally, the role of a pre-annealing process towards enhancing ductility was revealed [13]: AZ31 alloy sheet with weak basal texture had poor stretch formability upon rolling, but the opposite was observed when the sheets with strong basal textures. Therefore, the initial texture of the AZ31 alloy influences ductility.

Differential speed rolling (DSR) / Asymmetric rolling [14,15] is a rolling process where further increase in grain refinement can be achieved by inducing shear deformation during the rolling process. On the same basis, calibre rolling (also referred to as groove rolling or stretch pass rolling) could also be performed, where an AZ31 billet is rolled and reduced through a series of grooves [16-18]. During the processing, the reduction direction is changed over each pass by rotating the billet 90°, facilitating the formation of an equiaxed microstructure. When AZ31 alloy was calibre rolled at high temperatures such as 723 K, exceptional ductility was observed due to texture strengthening [18]. Thus, it is believed to be an economical and efficient process for the production of Mg alloys in the form of bars.

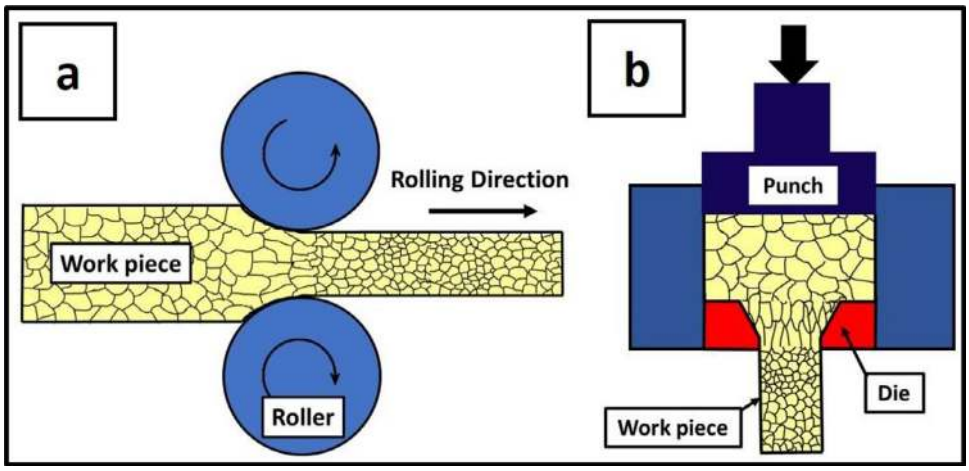

Fig. 1. Schematic illustration of a). Rolling Process, and b). Extrusion Process.

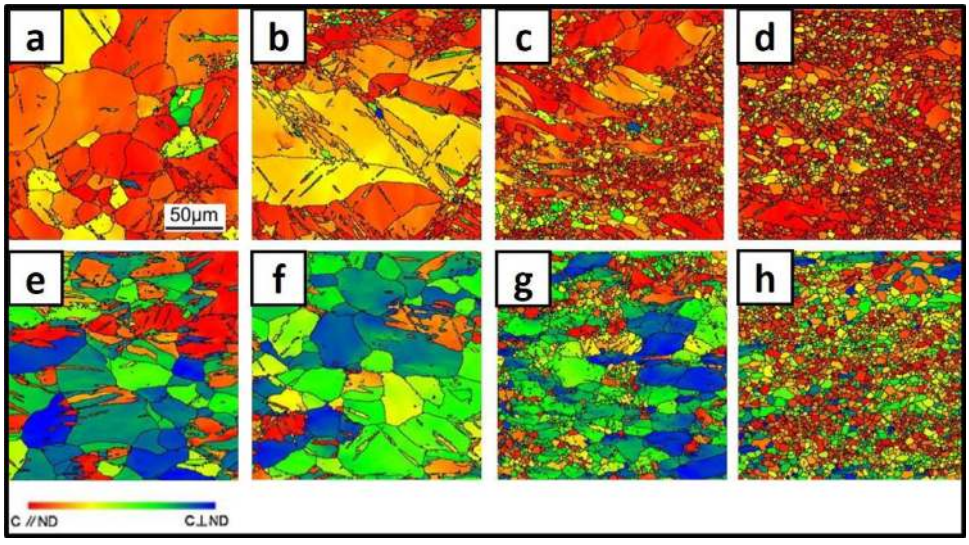

Fig. 2. Orientation image maps illustrate the angles between the c-axis and Normal Direction of the sheet AZ31 alloy rolled at different reductions rates, in Normal Direction (a-d) and Transverse Direction(e-h): (a) and (b) 10%; (c) and (d) 20%; (e) and (f) 30%; (g) and (h) 40%. [11]. (For interpretation of the references to colour in this figure legend, the reader is referred to the web version of this article.)

2.1.2. Cold rolling

Cold rolling process is usually carried out below the recrystallization temperature of a particular metal [9]. The thermo-mechanics involved behind cold rolling is different compared to hot rolling. In the same way, controlling parameters such as the number of passes, and rolling speed have a different effect on the material property [6,19,20]. As discussed earlier, Mg deforms only by basal slip, which consequently increases with the applied loads. This is achieved through an increase in the reduction% of the rolled sheet. However, Mg alloys develop failures such as edge cracks and even fractures at reduction rates as low as 15% [19-21]. So, the number of passes and the reduction% need to be tailored carefully for a particular temperature.

The rolling speed, however, proved to have a considerable effect in grain refinement [10]. It was evident that high-speed rolling involves less heat transfer from the work piece to the roller. And higher temperatures imparted in AZ31 alloy through plastic strain subsequently decrease the requisite strain for DRX to occur. This induced more grain refinement and activation of $\langle c+a \rangle$ slip systems [19,22,23]. In low-speed rolling, however, deformation energy is accumulated and strong basal texture is formed at the surface. And an inhomogeneous deformation microstructure was developed in AZ31 alloy, leading to poor ductility characteristics and defects. Thus, a cross-rolling process could be performed at adequate conditions, before cold rolling [15]. The intense basal textures are then weakened, as a result of the interaction of deformation mechanisms and DRX. Such interactions can also be produced by shear deformation through asymmetric cold rolling. A weak basal texture and with significantly improved tensile-ductility is achieved [13,24].

Similarly, DSR with a roll speed ratio of 3:1 resulted in good isotropy of strength and excellent elongation characteristics [24]. These texture weakening attributes were also observed when AZ31 bars are calibre-rolled at cold working

temperatures [16,25]. And studies have been conducted in modifying these grooves to ensure uniform deformation and isotropy across the cross-section of a rolled bar [26,27]. However, increasing calibre rolling strain gives rise to a unique split of basal poles owing to the alternating loading axis [25]. This split texture is unique to calibre-rolled Mg alloys [28]. Nonetheless, these bars are usually subjected to annealing, as it is crucial to modulate the strength-ductility balance. As such, Kong et al. [25], investigated the effects of subsequent annealing process at different temperature regimes on the mechanical behaviour of calibre-rolled AZ31 alloy. When annealed at low temperatures (373–473 K), a decrease in strength and hardness was observed but ductility of the initial calibre-rolled alloy was preserved. Conversely, annealing at high temperatures (573–673 K), promotes grain growth but deteriorates all mechanical properties, thereby degrading the strength-ductility balance. This reduction in strength and hardness could be explained in light of the Hall-Petch relation. And the decrease in ductility could be justified from the activation of mechanical twinning that induced a highly localized shear deformation and strain incompatibility.

Furthermore, the application of three-high skew rolling process (also referred to as radial-shear rolling or cross-screw rolling) allows the production of AZ31 alloy bars with higher elongation in a single pass. Also, this process is capable of producing a final product with high straightness, low ovality and fewer surface defects, when compared to the calibre-rolling process [26,29,30]. In this process, the work piece is deformed plastically by drive rollers rotating in the same manner, whose axes are inclined to the rolling axis (18° commonly preferred for AZ31 alloy). Hence, the metal undergoes helical flow along a spiral trajectory, causing densification across the entire cross-section of the rolled bar and forming a tangential stress component along the periphery [31]. As such, microstructure refinement is primarily influenced by increasing rolling speed as they activate additional deformation mechanisms. Doing so leads to higher band twist in the deformation zone, which intensifies the tangential stress component and redundant strain, causing microstructure refinement. Here, a bimodal grain structure was observed between the periphery (high strain intensity) and the axial zone (low strain intensity) of the rolled bar, thus leading to a non-uniform microhardness distribution [26]. And, it could be inferred that the periphery is composed of fine grains relative to the axial zone. The constructive interplay between these fine grain structures and activation of non-basal slip systems, enables three-high skew rolled AZ31 bars to have significant tensile strength and yield strength. However, both calibre rolling [16,17] and three-high skew rolling processes [30,31] have proven to be effective methods for obtaining fine grain sizes comparable to those obtained from SPD techniques.

2.1.3. Cryogenic rolling

Rolling process performed when the work piece has undergone cryogenic treatment at temperatures below 83 K [32,33] is commonly referred to as cryogenic or cryo rolling (CR). Since dynamic recovery is suppressed at cryogenic temperatures, grain refinement is further enhanced [34]. The effectiveness of CR on the strengthening of material is remarkably influenced by its stacking fault energy (SFE) [35,36]. With AZ31 alloy having an intermediate SFE, it deforms by twinning during CR, but dislocation slip during room temperature rolling. This makes CR the most effective over room temperature rolling in improving the strength.

As such, cryogenic treatment changes grain orientation in AZ31 alloy, attributing to frame-like twinning [33]. Further, the tensile strength and the hardness were higher than the untreated samples. This can be ascribed to the increased content of precipitated phases, like $Mg_{17}Al_{12}$, which strengthens the material [37,38]. Similar to other types of rolling, the initial texture of AZ31 alloy influences the twinning, microstructural and textural evolutions in the CR process [39]. After CR, UFGs were formed and the strength of the sample significantly increased. Although anisotropy is developed, where tensile strength along the rolling direction was higher than of the transverse direction. Unlike other deformation processes, the reduction percentage for AZ31 alloy in CR is only around 8% [40], as micro cracks and defects begin to develop along the grain boundaries. The variation of grain size, ultimate tensile strength, and elongation of AZ31 alloy, with respect to temperature and rolling reduction from various literature, are shown in Fig. 3 (a-c).

2.1.4. Extrusion

Extrusion is a metal forming technique performed to produce metals in various fixed cross-sectional profiles that cannot be achieved by rolling [9]. Here, a ram is made to push the billet through a die of the desired cross-section, as illustrated in Fig. 1(b). The die can be designed in such a way to produce complex profiles in a material without any draft. As a processing technique, extrusion can be used to tailor a billet material to have desired mechanical properties. Processing parameters such as temperature, extrusion rate (the rate at which the work piece is being extruded), and extrusion ratio (the ratio of the cross-sectional area of the work piece before and after extrusion) can greatly influence microstructure refinement [41-43]. Similar to the rolling process, the extrusion process is also generally classified by the materials working temperature: hot extrusion, and cold extrusion. However, cryogenic extrusion isn't feasible due to the limited workability of Mg towards the magnitude of extrusion forces. The following sub-sections will discuss how the respective processing parameters will influence the mechanical behaviour of AZ31 alloy upon extrusion.

2.1.5. Hot extrusion

Hot Extrusion process is carried out above the recrystallization temperature of a particular metal [9]. Here, parameters such as extrusion ratio, billet temperature, and ram speed have a great influence over microstructure refinement [41]. The effect of varying processing temperatures in the extrusion of AZ31 alloy is shown in Fig. 4(a-c) [42]. It is thus inferred that extrusion is easily performed at higher temperatures with the absence of work hardening effect, promoting

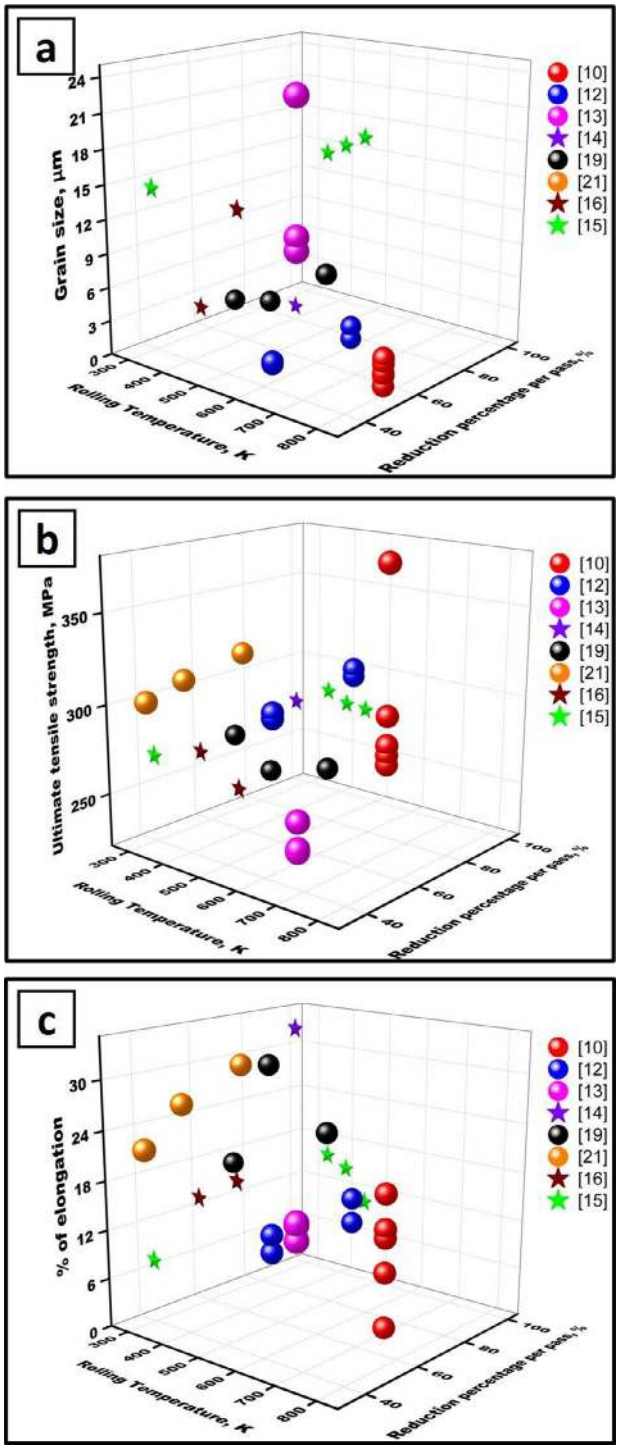

Fig. 3. 3D scatter plot showing the effect of rolling temperature and reduction percentage on AZ31 Magnesium alloys, a). Grain size, b). Ultimate tensile strength and, c).% of elongation. (Spheres- Symmetric Rolling; and Stars- Asymmetric Rolling). (For interpretation of the references to colour in this figure legend, the reader is referred to the web version of this article.)

DRX. Although grain growth is enhanced, an upper limit for billet temperature must be established to avoid effects such as oxidation, sintering, and hot shortness. This is done by observing the development of surface cracks. To address this, Hsiang et al. [43], stated that oxidation prevention methods must be considered at extruding at 673 K.

However, grain refinement seems to be influenced by the initial texture [40,41], as more elongation was observed in the AZ31 extrudate when the billet was initially homogenised at 673 K. This might be attributed to the dissolution of intermetallic compounds such as $Mg_{17}Al_{12}$ and Al_8Mn_5 in the billet at the time of cast. This also explains why a homogenised billet can be extruded faster than an as-cast billet. Nevertheless, the extrusion speed directly corresponds to the extrusion load, and a fixed speed throughout the process dramatically increases these loads and yield serious defects in AZ31 alloy [43]. With a multi-speed approach, even with a high extrusion ratio, loads are moderated within a shorter period, and a defect-free AZ31 alloy is obtained. Although only an extrudate processed at lower speeds obtain the finest grain size [41], which was parallel to the observation in Fig. 4(c-d) [42].

Further grain refinement can be attained by inducing more deformation by varying extrusion ratios and die designs [41,43-47]. As mentioned before, AZ31 alloy has good workability in high temperatures, and thus, high extrusion ratios ($\geq$39) [48] can be achieved easily [41]. In the die, various features can be implemented to promote shear deformation: particularly asymmetric extrusion feeders with an angled chamfer in one face [47], and asymmetrically tapered feeders [45]. This produces grain refinement and a tilted weak basal texture, which enhances room temperature strength and plasticity.

2.1.6. Cold extrusion

Cold or Warm Extrusion process is carried out below the recrystallization temperature of a particular metal [9]. In the absence of high temperatures, oxidation effects are less pronounced, and cold working induces greater strength in the extrudate. Only fewer studies have been carried out in cold extrusion of AZ31 alloy, as higher forces are required for deformation and the process is more expensive [49,50]. All related process parameters such as ram speed and extrusion ratio need to be chosen appropriately for a given temperature as they all have a direct influence over the load acting on the material.

A pre-extruded AZ31 billet with an oil-based graphite lubricant was used in a cold extrusion study which yielded grain sizes finer than of hot extruded AZ31 alloy [49]. Although at higher extrusion rates, and lower temperatures, surface cracks and defects are more common [50]. This provokes the usage of back pressure (BP) and a hydrostatic medium to extrude the metal. The application of BP allows the usage of higher extrusion ratios and extends the formability of AZ31 alloy. As such, strong elongated or even fibrous grains were produced. The adiabatic heating effect generated during deformation can be as high as 0.4–0.65 of the absolute melting temperatures, stimulating recovery, and DRX. The variation of grain size, ultimate tensile strength, and elongation of AZ31 alloy, with

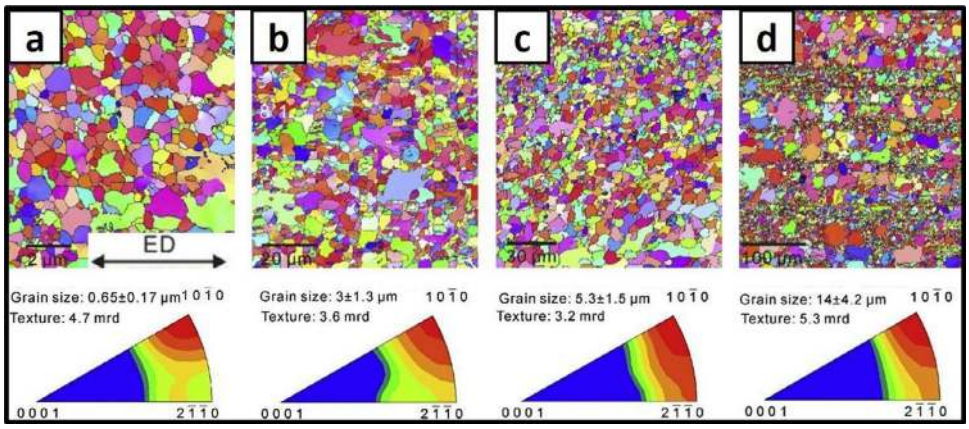

Fig. 4. Transmission Kikuchi Diffraction orientation maps and inverse pole figures of AZ31 along extrusion direction, extruded at (a) 175 °C, Electron Back Scatter Diffraction orientation maps and inverse pole figures along extrusion direction of AZ31 extruded at (b) 300 °C and (c) 400 °C with ram speed of 0.1 mm. s^{-1}, and (d) 400 °C with ram speed of 3 mm/s. [42].

respect to temperature and extrusion ratio from various literature, are shown in Fig. 5(a-c).

3. Severe plastic deformation

As established earlier, materials produced through the application of SPD offer the possibility of refining the grain size in the sub-micrometre range of 100–1000 nm or even in the true nanometre range of <100 nm, which are drastically smaller than those produced using conventional bulk-deformation techniques [51,52]. The techniques that fall under SPD can process a specimen without changing its cross-sectional dimensions. And the process introduces a high dislocation density in a material, which then rearrange into arrays of high-angle grain boundaries. This results in excellent homogeneity and mechanical properties which are in conjunction with the Hall-Petch relation [6,51]. Several different SPD techniques may exist [53] but for AZ31 alloy, but the most attention has been given to the procedures involving equal-channel angular pressing (ECAP) [54], Accumulative Roll Bonding (ARB) [55], and HPT [4], as schematically illustrated in Fig. 6.

3.1. Equal channel angular pressing

ECAP is a commonly used SPD technique producing materials with grains in the sub-micron range [51]. The working principles of ECAP are schematically depicted in Fig. 6(a). This shows that the process is operated in a die containing a channel bent by an angle near the centre of the die. The billet is machined to fit within the channel and a plunger is used to drive it through the die under applied pressure. And grain refinement occurs at the channel bend due to shear deformation, inducing exceptional mechanical properties.

In practice, the deformation introduced in AZ31 alloy is controlled by various parameters such as the working temperature, channel angle, number of passes, and the application of back-pressure [51,54,56–58]. Apart from this, experimental evidence shows that microstructural evolution depends upon how the sample is rotated between each pass: Route A- rotate 0°, Route B_A- rotate ±90°, Route B_C- rotate 90°, and Route C- rotate 180° [59–61]. Amongst them, pressing through route B_C is commonly preferred, since a regular and periodic restoration of the equiaxed structure is achieved and deformation is observed on all three orthogonal planes.

The underlying principle of ECAP is a sample being subjected to repetitive pressing to induce high strains. However, the imposed plastic strain is primarily decided by the number of passes. Also, it was found that a gradual decrease in grain size occurs with the increasing number of ECAP passes [62]. However, it was commonly observed that the material cannot undergo further grain refinement once DRX is completed. This could explain why grain size mostly remains unchanged after 4 passes for Mg alloys [62,63]. This number, however, changes with the type of process [64]. In AZ31 alloy, grain refinement is characterized by nucleation of a necklace-like pattern of fine grains surrounding a coarse grain in the initial pass, which will later be homogenised through further passes, irrespective of the billet being cast or wrought [54,58,65–67].

Thus, it was inferred that, by increasing the imposed plastic strain, UFG can be achieved which induces better mechanical properties. Nevertheless, as with any other processing technique, the temperature does play a vital role in ECAP. When performed at higher temperatures, higher activity of DRX is observed [62]. Despite better processing speed and workability, fine grain sizes couldn't be obtained. The specimens processed at elevated temperatures produce yield stress values lower than their as-cast form due to DRX and subsequent grain growth [58]. On the contrary, a significant increase in the yield stress was observed when the specimen was processed at room temperature. With grain refinement being primarily determined by DRX, it was informed that finer grain sizes can be obtained at lower temperatures [61,68].

Anyhow the threshold working temperature depends on the workability of the material to be processed [61]. Due to the lack of available slip systems in AZ31 alloy, the specimens easily form cracks or fail below 473 K during ECAP [68,69]. However, the usage of back-pressure provides the advantage

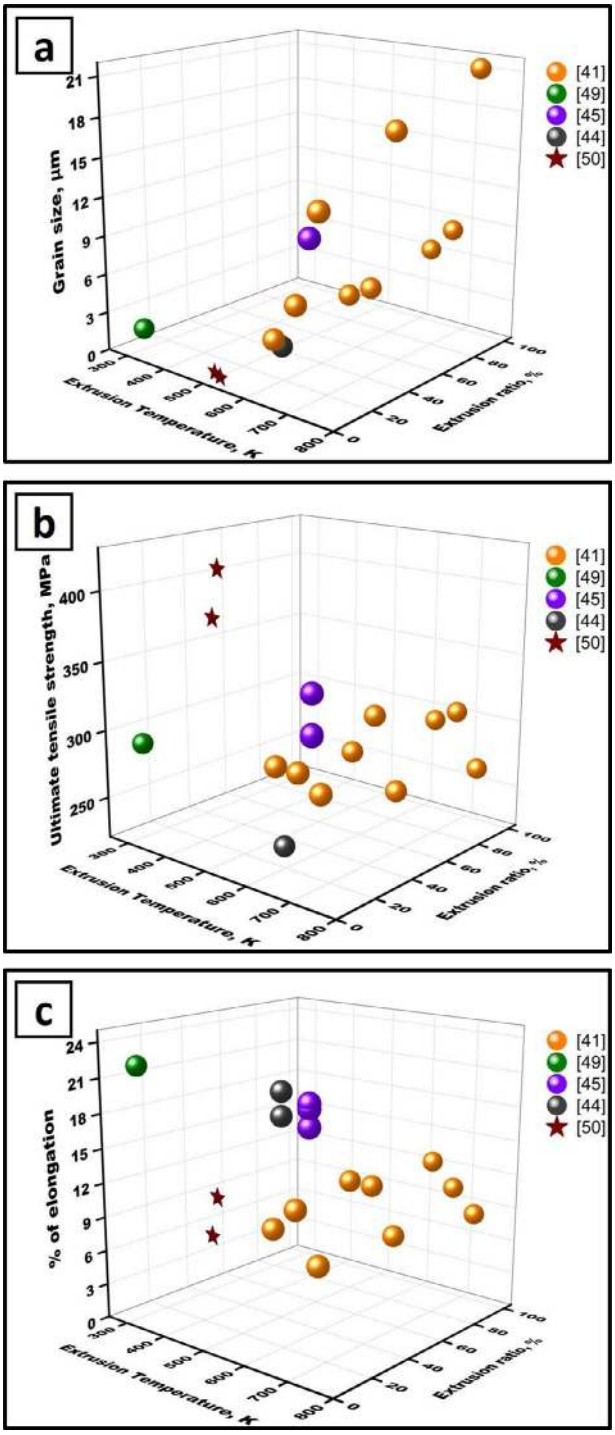

Fig. 5. 3D scatter plot showing the effect of Extrusion temperature and extrusion ratio on AZ31 Magnesium alloys, a). Grain size, b). Ultimate tensile strength and, c).% of elongation. (Spheres- Symmetric Extrusion; and Stars- Asymmetric Extrusion).

of pressing AZ31 alloy at lower temperatures, resulting in remarkable grain refinement. Though a bi-modal grain structure is formed initially, with the aid of multiple passes, it rapidly becomes homogeneous and grains reduce to the submicron range. In addition to that, grain refinement with the application of back-pressure has led to the development of superplastic capabilities when AZ31 alloy is tested in tension at elevated temperatures [54,70,71]. This can be attributed to the formation of bimodal microstructures, as larger grains can easily accommodate grain boundary sliding through intragranular slip and twinning [72-76]. The $<c+a>$ dislocations and $\langle c+a \rangle$ non-basal slip was prevalent with the use of back-pressure. This contributes to the strain hardening of AZ31 alloy and thus suppressing necking. This confirms that the highest level of super plasticity corresponds with the decrease in processing temperature and a concurrent increase in back-pressure.

The material behaviour could further be enhanced by varying the channel angle [51,61]. After considering the amount of deformation imposed, it could be inferred that the lesser the channel angle, the finer the grain size produced. But considering the workability of AZ31 alloy, various studies concluded that a 90° angled die induced maximum grain refinement with the least amount of defects. The arc of curvature or corner angle is also an important parameter since a sharp turn in the channel produces friction between the die and the material [54,65]. To avoid the formation of dead zones within the material flow, a corner angle of 20–30° is given while processing the AZ31 alloy.

Nonetheless, ECAP still won't be able to satisfy the demands of the manufacturing sector as it can't produce continuous billets [77,78]. This is because the friction developed in the channel is proportional to the length of the billet. After extensive FEA, a cyclic process named Incremental-ECAP (I-ECAP) was proposed [79]. This is done by separating the feeding and the plastic deformation stages of the conventional ECAP. Despite being a continuous SPD process and operating at temperatures around 500 K, I-ECAP was capable of producing large amounts of strains in AZ31 alloy, and mechanical properties similar to that of conventional ECAP [78–80]. Additionally, the working temperatures and processing routes are the most influential process parameters in I-ECAP for the resulting mechanical behaviour. The effect of processing AZ31 alloy through various routes in I-ECAP is shown in Fig. 7 [78].

3.2. High pressure torsion

HPT technique has a longer history than ECAP, as the outlying principle behind it was first proposed more than 70 years ago [81,82]. Although it was recognized as a tool for exceptional grain refinement only in the last two decades. It is capable of producing grains of the UFG range and sometimes even the nanocrystalline range (grain sizes less than 100 nm) making it the most effective of all SPD techniques [83]. In this process, the material is subjected to torsional shear straining with high hydrostatic pressure of 0–7 GPa [53,81-85]. Generally, the specimen is in the form of a disk located within a cavity between two anvils, as schematically illustrated in Fig. 6(b). And the process is usually conducted under quasi-constrained conditions [82], where a limited flow of material is allowed in between the upper and lower anvils. In practice, the HPT process begins with the disk being subjected to hydrostatic pressure for 30 s, which is commonly referred to as

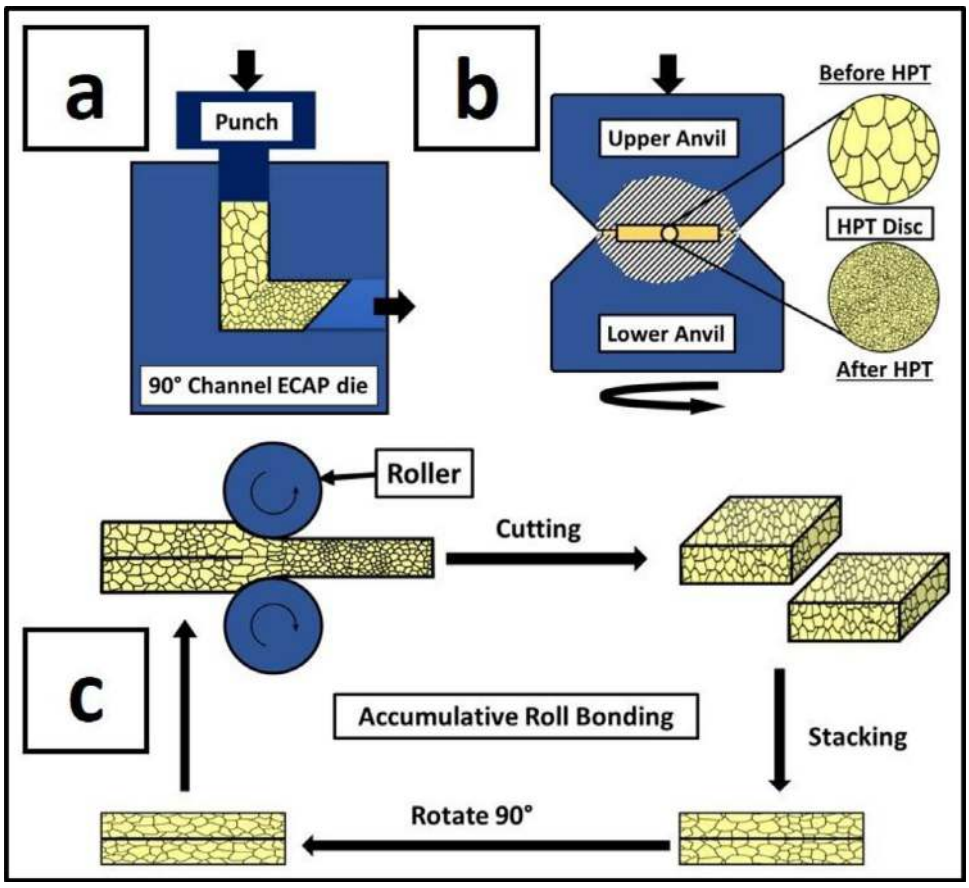

Fig. 6. Schematic illustration of SPD Processes, a). ECAP, b). HPT and, c). ARB.

the $N=0$ condition. The torsional straining is then induced by rotating one of the anvils. This causes shear deformation in the material, which initiates microstructure recrystallisation. However, the resulting grain size is influenced by processing parameters such as the working temperature, the pressure applied, number of rotations, and speed of rotation.

Amongst the various SPD processes, HPT is highly preferred for AZ31 alloy, as it can be performed at room temperature without any segmentation like in the ECAP process [68]. This is ascribed to the hydrostatic stress applied, which prevents the formation of these defects and increase workability. The torsional strain on the work piece is estimated using the number of anvil rotations N, which starts with 0, ¼, ½ and extends up to 20 turns [86-89]. The current author performed HPT on AZ31 alloy for the above-mentioned strains under 5 GPa pressure with 1 rpm speed, as shown in Fig. 8 [4]. It was observed that at N=¼ the grain refinement starts by sub grain formation and shear bands. This is parallel with other works of literature, where equilibrium grain size at the UFG range was achieved by 1 pass [4,86,90,91]. The presence of shear bands however indicates the presence of inhomogeneity of deformation, where grain sizes vary through the radii and thickness. This variation of grain sizes through the radii of the AZ31 disk is shown in Fig. 9 [86].

This, however, is mendable with an increasing number of turns, as microstructure becomes increasingly homogenous with higher dislocation densities and grain growth due to the heat generated through torsional straining. And as discussed earlier, the amount of hydrostatic pressure also influences the degree of microstructural refinement. With a pressure of 2.5 GPa, complete homogeneity of AZ31 alloy was achieved after $N=15$ [87]. However, the authors' work achieved the same amount of homogeneity with 5 GPa pressure and $N=5$ [4]. In addition, the working temperature is also an influential parameter for the resulting grain size. High-temperature processing results in grain growth and elongation due to pronounced DRX, while low temperatures processing induces significant grain refinement and hardness [85].

Moreover, processing with high hydrostatic pressure attributes to the superplastic behaviour in AZ31 alloy at $N=10$ [89]. This behaviour is prevalent as a result of grain boundary sliding controlled by grain boundary diffusion [89,92-95]. Maximum elongation of 520% was observed when the superplastic AZ31 specimen was tensile tested at 623 K [89]. Apart from this, the anvil's surface roughness also plays a vital role in sample homogenization. Due to limited slippage between the work and anvil, more strain was induced [89]. Further, Pauline et al. [96] performed HPT on AZ31 alloy

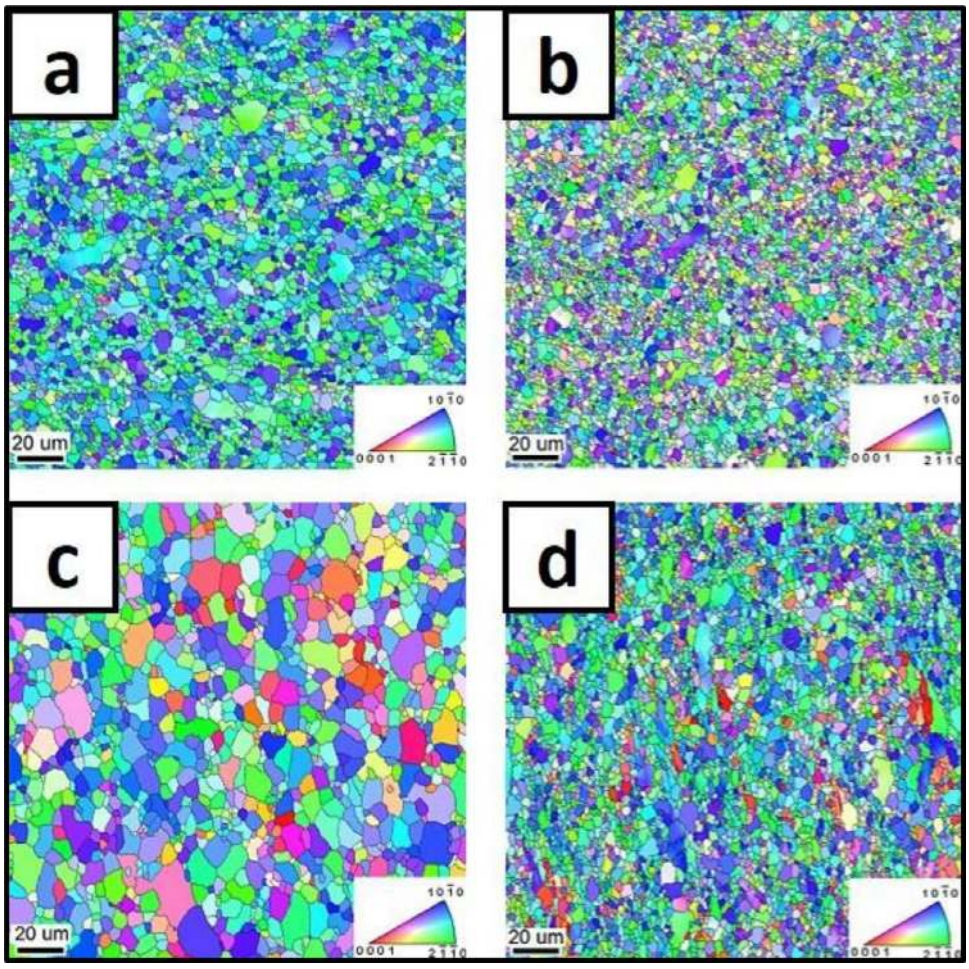

Fig. 7. Electron Back Scatter Diffraction maps and corresponding micro-textures of AZ31 alloy processed by I-ECAP at, a). 250 ° (route A), b). 200° (route A), c). 250 ° (route B_c), d). 200° (route B_c). [78].

at various strain rates. Through this study, it was observed that increasing strain rate causes a reduction in the grain size and consequently an increase in hardness. This is attributed to the decrease in ⟨a⟩ type prismatic and pyramidal fraction of dislocations [87,93].

3.3. Accumulative roll bonding

Accumulative Roll Bonding (ARB) is an SPD process, which can be accomplished by using the same facility as the rolling process [53,55]. It is a multi-stage process involving a series of rolling, cutting, brushing, and stacking, as schematically illustrated in Fig. 6(c). Commonly the sheet is reduced in thickness by 50% upon rolling and then bisected span wise. These two halves are then evenly stacked one over the other to be rolled again. This process is repeated till large strains are accumulated in the sheet and UFGs are produced.

The principle behind ARB is the Interface bonding, which is achieved by DRX at the sheets interface [97,98]. Here the fine grains are recrystallized and replaced until the interface is eliminated. Using ARB, AZ31 alloy sheets can be roll bonded to sheet metals of 3 types: similar materials [55,98–106], dissimilar materials [107–112] and, similar/dissimilar materials with reinforcing agent [113]. For all these types, however, the processing parameters exert their influence over the resulting material properties. These include the number of layers, reduction%, working temperature, rolling speed, and rolling friction.

The number of passes in ARB is crucial for homogenous UFG formation as revealed by the EBSD microstructure in Fig. 10 [99]. The grain size was observed to decrease drastically after one pass. Even though only bimodal structures were obtained at this point, AZ31 alloy showed a superior combination of high strength and good elongation. The ductility being attributed to non-basal slip and the strong back stress offered [104,106,114]. With further passes, more homogeneity is met in grain size distribution. This leads to the suppression of twin generation and reduction in mechanical anisotropy. Even while rolling dissimilar metals to AZ31 alloy, the diffusion layer thickens with the increasing number of passes [109,110].

This effect is also observed when the reduction percentage of AZ31 alloy is increased from 50%, resulting in an enhanced bonding area by the effect of high strain accumu-

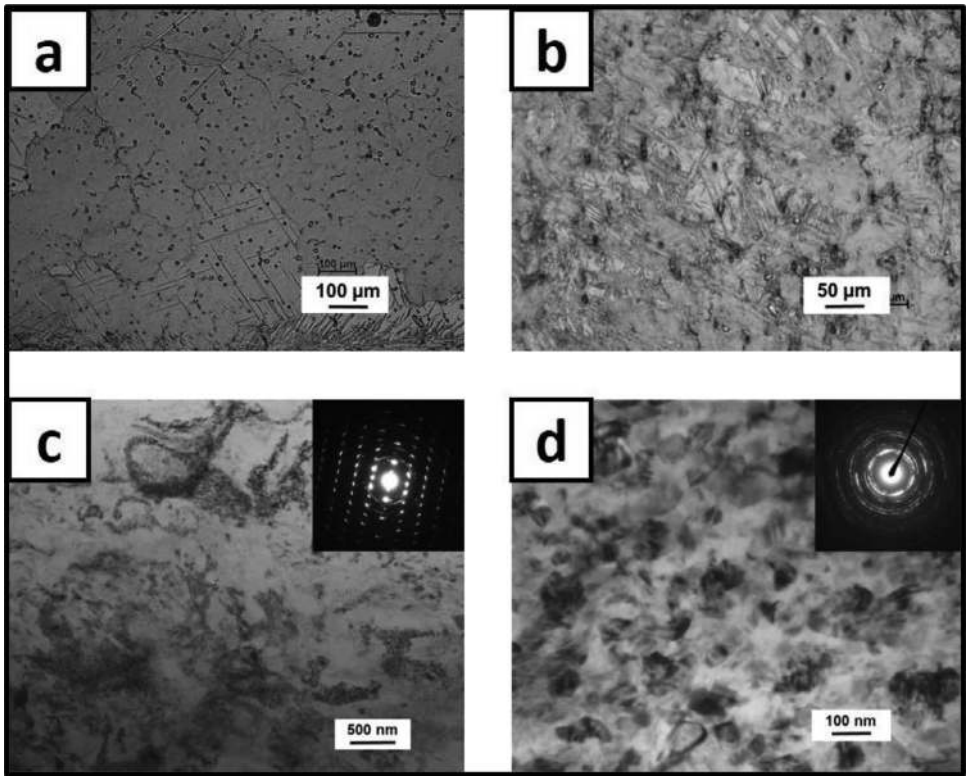

Fig. 8. Optical Microscope image of AZ31 Mg Alloy (a) as-cast and (b) HPT N = 0 samples, and Transmission Electron Microscope bright field images of HPT (c) N = ¼ and (d) N = 5 samples [4].

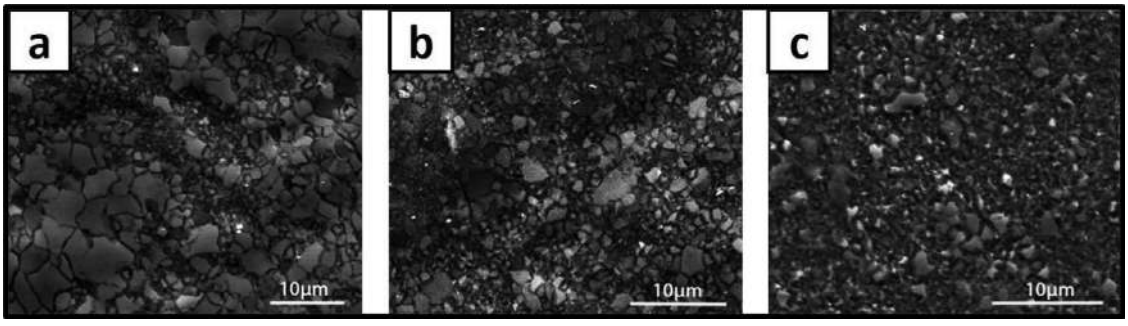

Fig. 9. Microstructures of AZ31 alloy after HPT processing at 473 K for N ¼ 1 turn at (a) the centre, (b) the half-radius, and (c) the edge of the disk [86].

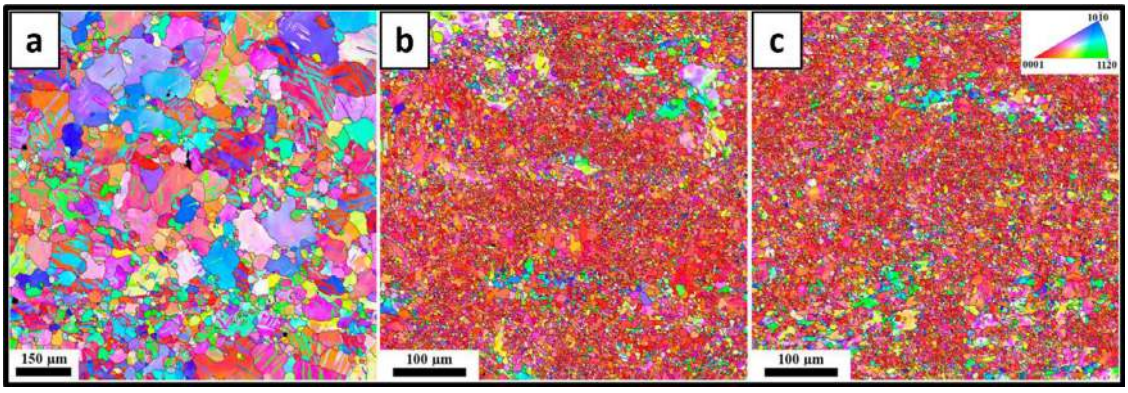

Fig. 10. Electron Back Scatter Diffraction microstructure of (a) Homogenised AZ31 alloy; and alloy processed through ARB after (b) first pass; and (c) second pass [99].

lation [107,108,110]. However, the finest grain sizes aren't produced with the highest reduction percentage [102]. This might occur due to inadequate preheat temperature, attributing incomplete DRX, and the residual accumulated strain energy. Fatemi et al. [55] took this into account, and mean grain size of 0.9 μm was achieved with an 85% reduction in a single pass.

Nevertheless, In ARB, the onset of DRX decides the level of grain refinement and forms shear bands in the direction of shear stress [98,112]. The best degree of refinement is achieved when the process temperature is low. High values of tensile strength, yield strength, and microhardness are also obtained. Although, increasing working temperatures have a direct effect on elongation, and formability index [55,100,111]. This is due to the higher number of nuclei created, which facilitates grain growth and formability. Although not many studies have been conducted on the effect of varying rolling speed, it is understood from a few studies that decreasing rolling speed results in stronger interface bonding [97-100]. This is attributed to the prolonged period of loads applied, to cause more DRX and diffusion. Bonding is also dependant on the friction between the rolls and the specimen, and between the interfaces [101]. Thus, wire-brushing operation between every ARB pass is done to remove oxides/any other surface layers, which improves the bonding quality.

Grain boundary subdivisions through the transition of low angle to high angle grain boundaries induced by the accumulated strain are one of the mechanisms that result in excellent great grain refinement with super plasticity [92,94,101]. Thus, super plasticity can be observed in the AZ31 alloy during hot tension tests. At 573 K and a slow strain rate of $10^{-4}\ s^{-1}$, superplastic elongations of about 562% were obtained [101]. Though testing the same specimen at a higher strain rate of $10^{-2}\ s^{-1}$, superplastic elongation was reduced to 316%. Taking into account the strain rate sensitivity exponent of 0.34, it can be inferred that grain boundary sliding plays a primary role in superplastic deformation. The variation of grain size in AZ31 alloy, with respect to working temperature from the literature of the above-discussed SPD techniques, are shown in Fig. 11. And the mechanical behaviour elicited through various process parameters of those techniques are given in Tables. 2-4.

3.4. Numerical methods and finite element analysis

An ideal processing technique must achieve the required refinement efficiently and reliably [2]. However, this is easier said than done, as a tremendous amount of energy and money must be spent in bulk processing AZ31 alloy. As such, Industries must rely on numerical methods/processing maps in choosing suitable process parameters. And with the advent of FEA, a more structured approach has been established [115,116]. By computationally simulating a processing technique, one can assess the thermo-mechanical behaviour of the material at any given condition. Further, a process optimization diagram can be generated through FEA without having to process any material [8]. Apart from obtaining an optimum set

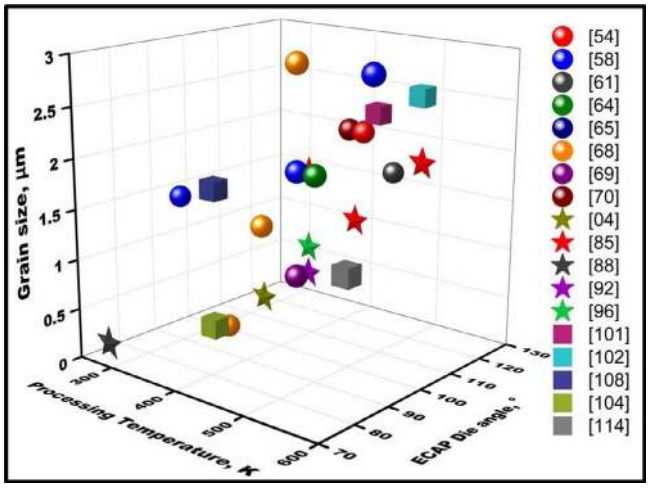

Fig. 11. Effect of processing temperature to the grain refinement of various SPD processes. (Sphere– ECAP after 4 passes; Star- HPT after 5 turns; Cube- ARB after 3 passes).

of process parameters, this data is crucial to establish threshold factors while processing to maintain workability and avoid any failure.

The metal is continuous throughout the process, for deformation techniques such as rolling and extrusion. Thus, the true strain experienced is based on the initial and final cross-sections of the work piece. This is represented in the Eq. (1) and (2) [117].

$$\epsilon = \ln \frac{t_0}{t_f}\ (for\ rolling\ ) \tag{1}$$

$$\epsilon\ = \ln \frac{A_0}{A_f}\ (for\ extrusion) \tag{2}$$

where, ϵ = true strain; t_0 = initial sheet thickness, mm; t_f = reduced sheet thickness, mm; A_0 = initial billet cross-sectional area, mm^2; and A_f = extruded billet cross-sectional area, mm^2. This is very useful in calculating the average flow stress of the material as it is the minimum stress a material requires to sustain plastic deformation. It is also useful to keep track of forming defects, as crack propagation is inversely proportional to the flow stress. The average flow stress is formulated in the Eq. (3) [117] given below,

$$Y_f = \frac{K\epsilon^n}{1+n} \tag{3}$$

where Y_f = average flow stress, MPa; K = strength coefficient (MPa); and n = strain hardening exponent (varies with material and working temperature). Thus, these values could be used to calculate the required rolling force, and the total power needed to rotate each roll mill using the Eq. (4) and (5) [117] respectively.

$$F = Y_f wL \tag{4}$$

$$P = 2\pi NFL \tag{5}$$

Table 2
Effect of ECAP processing parameters on the mechanical behaviour of AZ31 Mg Alloy.

ECAP												
S. No	**Die angle °**	**Ram speed mm. s^{-1}**	**Processing Temperature K**	**No. of pass**	**Grain size μm**	**Hardness HV**	**Yield Strength MPa**	**Ultimate Tensile Strength MPa**	**Strain %**	**Testing Temperature K**	**Strain Rate s^{-1}**	**Reference**
1	110	7	473	0	9.4	–	–	240	310	623	10^{-4}	[54]
				1	–	–	–	160	540			
				2	–	–	–	–	700			
				4	2.2	–	–	140	960			
2	90	0.25	298	0	450	–	60	–	–	298	10^{-3}	[58]
			473		–	–	65	–	–			
			573		–	–	50	–	–			
			298	1	–	–	120	–	–			
			473		–	–	100	–	–			
			573		–	–	50	–	–			
			298	4	1.5	–	210	–	–			
			473		–	–	65	–	–			
			573		–	–	20	–	–			
3	90	1.67	473	1	1.6	–	–	–	–	298	3×10^{-3}	[61]
				2	1.4	–	–	–	–			
				3	1.2	–	–	–	–			
				4	1.3	–	–	300	–			
				5	–	–	–	–	–			
				6	–	–	–	–	–			
	120	1.67		1	2.2	–	–	–	–			
				2	1.8	–	–	–	–			
				3	1.6	–	–	–	–			
				4	1.7	–	–	320	–			
				5	1.6	–	–	–	–			
				6	1.9	–	–	–	–			
		0.13		1	2.4	–	–	–	–			
				2	1.9	–	–	–	–			
				3	2	–	–	–	–			
				4	2.1	–	–	–	–			
				5	2.2	–	–	–	–			
				6	–	–	–	–	–			
4	90	0.28	498	1	4.1	–	–	–	–	–	–	[64]
				4	2.05	–	–	–	–			
				8	1.91	–	–	–	–			
5	120	–	573	0	26.7	53	–	200	–	–	–	[65]
				1	13.3	60	–	220	–			
				2	11.2	69	–	245	–			
				3	9.4	66	–	225	–			
				4	8	64	–	210	–			

(*continued on next page*)

Table 2 (*continued*)

ECAP												
S. No	**Die angle °**	**Ram speed mm. s^{-1}**	**Processing Temperature K**	**No. of pass**	**Grain size μm**	**Hardness HV**	**Yield Strength MPa**	**Ultimate Tensile Strength MPa**	**Strain %**	**Testing Temperature K**	**Strain Rate s^{-1}**	**Reference**
6	90	4	473	2	5.5	–	210	275	16	298	10^{-3}	[68]
				4	3	–	160	250	24			
				8	2	–	250	310	14			
		0.003	423	2	–	–	–	–	–			
				4	1.4	77.5	–	–	–			
				8	1	77.5	–	–	–			
			373	4	0.3	86	–	–	–			
7	90	0.003	473	1	–	87			25	–		[69]
				4	–	92			29			
				8	0.9	94			32			
8	110	–	453	4	2.2	–	–	–	100	623	10^{-1}	[70]
						–	–	–	200		10^{-2}	
						–	–	–	360		10^{-3}	
						–	–	–	960		10^{-4}	
						–	–	–	590	673	10^{-3}	
						–	–	–	900		10^{-4}	
			473			–	–	–	240	623	10^{-2}	
						–	–	–	600		10^{-3}	
						–	–	–	690		10^{-4}	
						–	–	–	280	673	10^{-2}	
						–	–	–	700		10^{-3}	
						–	–	–	1020		10^{-4}	
						–	–	–	200	723	10^{-1}	
						–	–	–	350		10^{-2}	
						–	–	–	650		10^{-3}	
						–	–	–	580		10^{-4}	
9	110	–	473	8	0.7	–	217	282	120	423	10^{-2}	[71]
					–	–	–	–	150		10^{-3}	
					–	–	–	–	460		10^{-4}	
					–	–	–	–	220	473	10^{-2}	
					–	–	–	–	280		10^{-3}	
					–	–	–	–	240		10^{-4}	
					–	–	–	–	200	523	10^{-2}	
					–	–	–	–	200		10^{-3}	
					–	–	–	–	120		10^{-4}	

(*continued on next page*)

[m5+;May 15, 2021;11:28]
Journal of Magnesium and Alloys xxx (xxxx) xxx

Table 2 (*continued*)

ECAP												
S. No	**Die angle °**	**Ram speed mm. s^{-1}**	**Processing Temperature K**	**No. of pass**	**Grain size μm**	**Hardness HV**	**Yield Strength MPa**	**Ultimate Tensile Strength MPa**	**Strain %**	**Testing Temperature K**	**Strain Rate s^{-1}**	**Reference**
10	90	15–20	473	6	3.2	–	–	–	280	490	10^{-4}	[72]
						–	–	–	380	550		
						–	–	–	560	623		
						–	–	–	320	623	10^{-3}	
						–	–	–	140	623	10^{-2}	
				5		–	–	–	190	490	10^{-4}	
						–	–	–	280	550		
						–	–	–	350	590		
						–	–	–	420	610		
						–	–	–	580	623		
						–	–	–	200	623	10^{-3}	
						–	–	–	100	623	10^{-2}	
				4		–	–	–	250	490	10^{-4}	
						–	–	–	350	550		
						–	–	–	550	623		
						–	–	–	270	623	10^{-3}	
						–	–	–	140	623	10^{-2}	
			453	6		–	–	–	320	490	10^{-4}	
						–	–	–	360	550		
						–	–	–	960	623		
			423		~1	–	–	–	1200	623		
11	90	4	553	6	4.1	–	–	–	–	298	3.3×10^{-4}	[75]

Table 3
Effect of HPT processing parameters on the mechanical behaviour of AZ31 Mg Alloy.

HPT												
S.no	**Load**	**Speed**	**Processing Temperature**	**No of Turns**	**Grain Size**	**Hardness**	**Yield Strength**	**Ultimate tensile strength**	**Strain**	**Testing Temperature**	**Strain Rate**	**Reference**
	GPa	**RPM**	**K**		**μm**	**HV**	**MPa**	**MPa**				
1	5	1	298	0	–	80	–	–	–		–	[4]
				1/4.	–	100	–	–	–		–	
				5	0.115	125	–	–	–		–	
2	6	1	296	1	1.1	95	–	–	–		–	[85]
				5	1.36	105	–	–	–		–	
			373	1	1.03	90	–	–	–		–	
				5	0.93	100	–	–	–		–	
			473	1	1.53	65	–	–	–		–	
				5	1.7	75	–	–	–		–	
3	2.5	0.1	298	1/4.	0.9	95	–	–	–		–	[87]
				1/2.	–	100	–	–	–			
				1	–	105	–	–	–			
				3	–	–	–	–	–			
				5	0.2–0.3	105	–	–	–			
				15	0.15–0.2	110	–	–	–			
4	2.5	0.1	298	1/4.	–	∼100	–	–	–		–	[88]
				1/2.	–	∼100	–	–	–			
				1	–	∼100	–	–	–			
				3	–	–	–	–	–			
				5	–	105	–	–	–			
				15	0.1	110	–	–	–			
				1/4.	–	97						
				1/2.	–	93						
				1/4.	–	104						
				1/2.	–	97						
				1/4.	–	108						
				1/2.	–	103						
				1	–	85						
				1/2.	–	107						
				1	–	100						
				1	–	102–109						
5	7	1	298	2		90			240	623	10^{-3}	[89]
									320	623	3×10^{-4}	
									330	623	10^{-4}	
									370	673	10^{-3}	
									380	673	3×10^{-4}	
				10		100			280	623	10^{-3}	
									380	623	3×10^{-4}	
									520	623	10^{-4}	
									410	673	10^{-3}	
									440	673	3×10^{-4}	

(*continued on next page*)

Table 3 (*continued*)

HPT												
S.no	**Load**	**Speed**	**Processing Temperature**	**No of Turns**	**Grain Size**	**Hardness**	**Yield Strength**	**Ultimate tensile strength**	**Strain**	**Testing Temperature**	**Strain Rate**	**Reference**
	GPa	**RPM**	**K**		**μm**	**HV**	**MPa**	**MPa**				
6	6	1	298	1/4.	–	100	–	120	174	423	10^{-3}	[92]
							–	70	223	473		
							–	50	213	523		
				1	0.25	110	–	100	252	423		
							–	65	229	473		
							–	50	203	523		
				5	0.2	120	–	80	308	423		
							–	58	243	473		
							–	50	207	523		
				10	0.11	125	–	78	355	423		
								55	310	473		
								50	195	523		
7	6	1	298	20	–	–	–	270	–	373	10^{-2}	[93]
					–	–	–	230	60	373	10^{-3}	
					–	–	–	190	240	373	10^{-4}	
					–	–	–	180	280	373	10^{-5}	
					–	–	–	190	200	423	10^{-2}	
					–	–	–	130	280	423	10^{-3}	
					–	–	–	90	280	423	10^{-4}	
					–	–	–	60	300	423	10^{-5}	
					–	–	–	160	240	473	10^{-2}	
					–	–	–	90	240	473	10^{-3}	
					–	–	–	60	360	473	10^{-4}	
					–	–	–	40	480	473	10^{-5}	
8	6	0.1	298	1/2.	–	100	–	–	–		–	[94]
				1	–	116	–	–	–			
				2	–	117	–	–	–			
				3	–	115	–	–	–			
				5	–	115	–	–	–			
				7	–	115	–	–	–			
9	6	0.5	298	5	~0.5	85	–	–	–		–	[96]
		1				85–90	–	–	–			
		2				90	–	–	–			

[m5+;May 15, 2021;11:28]
Journal of Magnesium and Alloys xxx (xxxx) xxx

Table 4
Effect of ARB processing parameters on the mechanical behaviour of AZ31 Mg Alloy.

ARB												
S. no	**Reduction%**	**No of cycles**	**Speed RPM**	**Processing Temperature K**	**Grain size μm**	**Hardness HV**	**Yield Strength MPa**	**Ultimate Tensile Strength MPa**	**Strain %**	**Testing Temperature K**	**Strain rate s^{-1}**	**References**
1	50	1		673	~10	–	–	350–360	–	296		[99]
						–	–	290–300	-	373		
						–	–	120–150	–	473		
						–	–	40–40	–	773		
		2			~7.6	–	–	360–370	–	296		
						–	–	290–280	–	373		
						–	–	100–100	–	473		
						–	–	40–40	–	773		
2	80	1	48	623	4	–	–	–	–			[101]
		2			3	–	–	–	–			
		3			2.8	–	–	–	570	573	10^{-4}	
						–	–	–	400	573	10^{-3}	
						–	–	–	316	573	10^{-2}	
						–	–	–	290	573	10^{-1}	
3	80	1	52	673	4.2	–	–	–	–			[102]
		2			~3	–	–	–	–			
		3			~3	–	–	–	–			
		4			3	–	–	–	–			
4	50	1		573	–	73	225.9	303	25.1	Room		[108]
		2			–	77	231.5	308	21.4	Temperature		
		3			2.4	80	236	315	19.6			
5	50	2	45	723	–	74.77	–	–	–	–		[114]
		3			–	78.83	–	–	–			
		4			–	82.06	–	–	–			
		5			–	86.68	–	–	–			
		6			–	87.63	–	–	–			
		7			–	89.29	–	–	–			
		8			0.35	93.61	–	–	–			
6	50	3	23	573	1.3	–	–	–	–	–		[104]

where F = rolling force, N; w = the width of work to be rolled, mm; L = length of contact between the rolls and work, m; P = total power, J/s; and N = rotational speed, rpm. But unlike rolling, the extrusion process can be used to produce various cross-sections of an initial AZ31 billet. Thus, the effect of die shape is usually considered while calculating the total ram pressure required for extrusion to occur. The shape factor for a given design can be calculated by the Eq. (6) [117], and for a requisite value of flow stress, the extrusion pressure can be calculated by Eq. (7) [117].

$$K_x = 0.98 + 0.02\left(\frac{C_x}{C_c}\right)^{0.25} \tag{6}$$

$$p = K_x Y_f\left(\epsilon + \frac{2L}{D_0}\right) \tag{7}$$

where K_x = shape factor; C_x = perimeter of the extruded cross-section, mm; C_c = perimeter of a circle of the same the extruded cross-section, mm; p = extrusion pressure, MPa; L = length of billet needed to be extruded, mm; and D_0 = initial diameter of the billet, mm. The above-discussed parameters are essential for making finite element models for a given deformation process.

Using FEA, cases such as roll wear damage [118], and frictional behaviour [119–121] could be evaluated by monitoring local contact pressure and local sliding. Similarly, various simulations have been performed in extrusion for a range of conditions [122,123]. Using DEFORM-3D software, process optimization diagrams can be generated for a desired property in the AZ31 extrudate. The velocity flow fields obtained from the simulation are useful in detecting any possible network of micro-cracks [123]. However, for evaluating microstructural behaviour crystal plasticity models are required. Walde et al. [124], implemented a model (including the effects of crystallographic slip, recrystallization, and twinning [125,126]) in the ABAQUS software illustrating texture evolution of AZ31 alloy during hot rolling. At present, the cellular automata (CA) model [127] has overcome all shortcomings in evaluating grain size morphology, where material properties are mapped from finite element nodes to a number of CA arrays. It was understood from Fig. 12 [127], that the established CA model can accurately predict the microstructural evolution of AZ31 alloy upon hot deformation.

However, the initial boundary conditions for SPD techniques cannot be evaluated by the change in cross-sectional dimensions since they always remain uniform. Therefore, numerical methods surrounding its processing parameters rely on the accumulated strain in the work. For the ECAP process, the effective strain ε after N passes is calculated using the Eq. (8) [128,129].

$$\varepsilon = \frac{N}{\sqrt{3}}\left\{2\cot\left\{\frac{\phi}{2} + \frac{\psi}{2}\right\} + \psi cosec\left\{\frac{\phi}{2} + \frac{\psi}{2}\right\}\right\} \tag{8}$$

where ϕ = channel angle; and ψ = corner angle. Using the finite element code in DEFORM-3D software, FEA has been performed to study the deformation behaviour for applied strains associated with various channel angle and die angle configurations [130,131]. With AZ31 alloy being hypothesized as a rigid plastic element, friction between the work and tool interface plays an important role in the plastic deformation [132]. This was inferred by varying the amount of lubrication, where the required extrusion force increased proportionally with the apparent friction coefficient. Similar studies related to frictional behaviour have also been performed for I-ECAP [133-134]. The die design must also be thought of by simulating pressing at various temperatures and fillet angles. This results in better precision, stiffness, and tool life [135].

Unlike other SPD processes, HPT permits a defined continuous variation of strain in a single cycle. Since the applied torque exerted can be easily computed through the angle of rotation, the effective strain ε can be estimated by Eq. (9) [87,126],

$$\varepsilon = \frac{2}{\sqrt{3}}\frac{\pi N r}{h} \tag{9}$$

where N = number of turns; r = radius of the disk; and h = thickness of the disk. Even though no FEA studies of AZ31 alloy has been performed yet, simulations performed on other materials could still draw various conclusions [136–139]. With the DEFORM-2D and 3D software, flow behaviour, temperature evolution, stress, and strain distributions can be evaluated for various sets of loading conditions under unconstrained, quasi-constrained, and constrained conditions. It was also noted that the effect of friction was more pronounced compared to that of ECAP processes, and dissimilar friction coefficients at the top and bottom anvils have a prominent effect on strain gradients through the work piece thickness [140].

Analogous to ECAP, the accumulated strain during every pass is essential to model ARB [99,126,136]. The effective strain for N passes in ARB can be calculated by Eq. (10) [99].

$$\epsilon = \frac{2N}{\sqrt{3}}\ln\left(\frac{1}{1-r}\right) \tag{10}$$

where r = reduction ratio per pass. However, not many studies [141–143] have been conducted in ARB for AZ31 alloy since intermediate stages of cutting, stacking, and roughening is difficult to model. Although a single cycle ARB process was simulated in ABAQUS, considering the effect of friction, and the corresponding heat generation [136]. The influence of working temperature and friction conditions was observed through the strain distribution through the AZ31 sheet thickness. Nevertheless, a new experimentally validated model was developed for AA1050 alloy where ARB simulations were performed for 5 cycles [142]. Here, cutting and stacking operation has been realised using the mesh mapping solution in ABAQUS. The deformed mesh of a single passed sheet was mapped towards two different sheet geometries, which is then integrated into a single sheet before the next cycle.

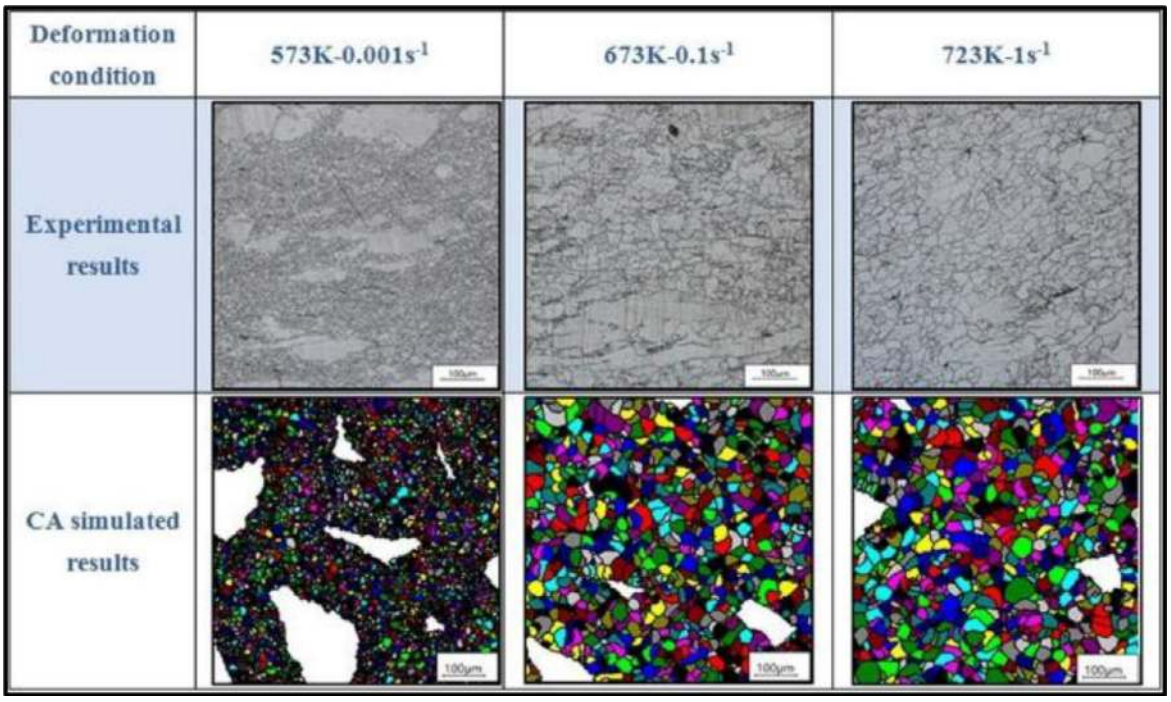

Fig. 12. The CA predicted grain size morphology of AZ31 Mg alloy after hot deformation at (a) 573 K - 0.001 s^{-1}; (b) 673 K - 0.1 s^{-1}; (c) 723 K - 1 s^{-1}. [127]. (For interpretation of the references to colour in this figure legend, the reader is referred to the web version of this article.)

4. Summary

The discussion above elaborates on various bulk-processing techniques and its respective process parameters. And these fine-grained or UFG materials with critical mechanical properties such as high specific strength, and good fatigue life, are vital to the advancement of the automobile and aerospace industry. As such, these techniques can be used to achieve significant grain refinement, homogeneity, and hardening of AZ31 alloy.

Under bulk deformation techniques, the highest levels of grain refinement and mechanical properties were achieved by performing asymmetric rolling, calibre rolling and three-high skew rolling. Whereas amongst SPD techniques, HPT presented the prospect of processing AZ31 alloy at room temperatures, and grains refined to the nano-range. However, only a few studies have explored the effects of combining multiple processing techniques in AZ31 alloy: enhanced tensile strength and ductility upon undergoing both ECAP and rolling [144,145], and the production of high-strength micro-gears by combining ECAP and extrusion [146].

Nevertheless, all SPD techniques are capable of producing an equiaxed UFG microstructure and superplastic elongation in AZ31 alloy. Thus, there is more attention is towards viable continuous production methods of UFG materials. Using Finite-Element methods, the machinery behind these techniques could be designed and optimum processing parameters can be obtained for the desired mechanical property in AZ31 alloy. As I-ECAP was computationally verified and performed for AZ31 alloy, more feasibility studies can be conducted for various continuous processing techniques such as Incremental-HPT, Single-Task Incremental HPT, and Accumulative Extrusion [128].

Amongst Monte Carlo, Sphere growth, Inverse analysis, and various other methods used to represent microstructure evolution, the CA finite element method has been very successful in modelling Static and Dynamic recrystallization phenomenon [147]. With only limited studies being performed, there is still of potential with the CA finite element method, to predict grain size morphology of AZ31 alloy using SPD techniques.

References

[1] ASM International Handbook Committee, Properties and selection: nonferrous alloys and special-purpose Materials was, ASM Int 2 (1990) 3470 http://books.google.com.hk/books?id=eC-Zt1J4oCgC.
[2] Gupta, M., Sharon, N.M.L. (2010). Magnesium alloys. In Magnesium, Magnesium Alloys, and Magnesium Composites (eds M. Gupta and N.M.L. Sharon). doi:10.1002/9780470905098.ch3.
[3] H.E. Friedrich, B.L. Mordike, Magnesium Technology, 2006.
[4] P. Seenuvasaperumal, K. Doi, D.A. Basha, A. Singh, A. Elayaperumal, K. Tsuchiya, Wear behavior of HPT processed UFG AZ31B magnesium alloy, Mater. Lett. (2018), doi:10.1016/j.matlet.2018.05.076.
[5] L.L.C. Catorceno, H.F.G. de Abreu, A.F. Padilha, Effects of cold and warm cross-rolling on microstructure and texture evolution of AZ31B magnesium alloy sheet, J. Magnes. Alloy. 6 (2018) 121–133, doi:10.1016/j.jma.2018.04.004.
[6] E.O. Hall, The deformation and ageing of mild steel: II Characteristics of the Lüders deformation, Proc. Phys. Soc. Sect. B. 64 (1951) 742–747, doi:10.1088/0370-1301/64/9/302.
[7] Q. Wei, S. Cheng, K.T. Ramesh, E. Ma, Effect of nanocrystalline and ultrafine grain sizes on the strain rate sensitivity and activation volume: fcc versus bcc metals, Mater. Sci. Eng. A. 381 (2004) 71–79, doi:10.1016/j.msea.2004.03.064.

[8] G. Liu, J. Zhou, J. Duszczyk, Process optimization diagram based on FEM simulation for extrusion of AZ31 profile, Trans. Nonferrous Met. Soc. China (English Ed. 18 (2008) s247-s251. doi:10.1016/s1003-6326(10)60211-7.
[9] E.P. Degarmo, R.A. Kohser, B.E. Klamecki, Materials and processes in manufacturing, J. Manuf. Syst. 17 (1998) 235, doi:10.1016/s0278-6125(98)80067-8.
[10] F. Guo, D. Zhang, X. Yang, L. Jiang, S. Chai, F. Pan, Influence of rolling speed on microstructure and mechanical properties of AZ31 Mg alloy rolled by large strain hot rolling, Mater. Sci. Eng. A. 607 (2014) 383–389, doi:10.1016/j.msea.2014.04.024.
[11] M. Wang, R. Xin, B. Wang, Q. Liu, Effect of initial texture on dynamic recrystallization of AZ31 Mg alloy during hot rolling, Mater. Sci. Eng. A. 528 (2011) 2941–2951, doi:10.1016/j.msea.2010.11.069.
[12] F. Guo, D. Zhang, X. Yang, L. Jiang, S. Chai, F. Pan, Effect of rolling speed on microstructure and mechanical properties of AZ31 Mg alloys rolled with a wide thickness reduction range, Mater. Sci. Eng. A. 619 (2014) 66–72, doi:10.1016/j.msea.2014.09.024.
[13] T. Zhou, Z. Yang, D. Hu, T. Feng, M. Yang, X. Zhai, Effect of the final rolling speeds on the stretch formability of AZ31 alloy sheet rolled at a high temperature, J. Alloys Compd. 650 (2015) 436–443, doi:10.1016/j.jallcom.2015.08.005.
[14] W.J. Kim, J.B. Lee, W.Y. Kim, H.T. Jeong, H.G. Jeong, Microstructure and mechanical properties of Mg-Al-Zn alloy sheets severely deformed by asymmetrical rolling, Scr. Mater. 56 (2007) 309–312, doi:10.1016/j.scriptamat.2006.09.034.
[15] H. Watanabe, T. Mukai, K. Ishikawa, Effect of temperature of differential speed rolling on room temperature mechanical properties and texture in an AZ31 magnesium alloy, J. Mater. Process. Technol. 182 (2007) 644–647, doi:10.1016/j.jmatprotec.2006.08.010.
[16] A. Singh, H. Somekawa, T. Inoue, T. Mukai, Evolution of microstructure during caliber rolling of AZ31 alloy, Magnes. Technol. (2013) 317–322, doi:10.1007/978-3-319-48150-0_53.
[17] J.H. Lee, B.J. Kwak, T. Kong, S.H. Park, T. Lee, Improved tensile properties of AZ31 Mg alloy subjected to various caliber-rolling strains, J. Magnes. Alloy. 7 (2019) 381–387, doi:10.1016/j.jma.2019.06.002.
[18] A. Tripathi, S.V.S.N. Murty, P.R. Narayanan, Microstructure and texture evolution in AZ31 magnesium alloy during caliber rolling at different temperatures, J. Magnes. Alloy. 5 (2017) 340–347, doi:10.1016/j.jma.2017.07.001.
[19] H. Kon, T. Sakai, H. Utsunomiya, S. Minamiguchi, Deformation and texture evolution during high-speed rolling of AZ31 magnesium sheets, Mater. Trans. 48 (2007) 2023–2027, doi:10.2320/matertrans.L-MRA2007875.
[20] M.R. Barnett, M.D. Nave, C.J. Bettles, Deformation microstructures and textures of some cold rolled Mg alloys, Mater. Sci. Eng. A. 386 (2004) 205–211, doi:10.1016/j.msea.2004.07.030.
[21] H.T. Jeong, T.K. Ha, Texture development in a warm rolled AZ31 magnesium alloy, J. Mater. Process. Technol. (2007) 559–561 187-188, doi:10.1016/j.jmatprotec.2006.11.084.
[22] J.W. Fergus, B. Mishra, D. Anderson, E.A. Sarver, N.R. Neelameggham, Improvement Of Low Temperature Formability Of Az, 31, 31 (2015) 209-217.
[23] Y. Onuki, K. Hara, H. Utsunomiya, J.A. Szpunar, High-Speed Rolling of AZ31 Magnesium Alloy Having Different Initial Textures, J. Mater. Eng. Perform. 24 (2015) 972–985, doi:10.1007/s11665-014-1318-8.
[24] M. Kaseem, H.W. Yang, K. Hamad, Y.G. Kim, B.H. Park, Y.G. Ko, Microstructure and plastic anisotropy of fine grained AZ31 magnesium alloy fabricated by differential speed rolling at 473 and 573 K, Mater. Res. Innov. 19 (2015) S5477–S5480, doi:10.1179/1432891714Z.0000000001135.
[25] T. Kong, B.J. Kwak, J. Kim, J.H. Lee, S.H. Park, J.H. Kim, Y.H. Moon, H.S. Yoon, T. Lee, Tailoring strength-ductility balance of caliber-rolled AZ31 Mg alloy through subsequent annealing, J. Magnes. Alloy. 8 (2020) 163–171, doi:10.1016/j.jma.2019.11.005.
[26] A. Stefanik, P. Szota, S. Mróz, T. Bajor, H. Dyja, Properties of the AZ31 magnesium alloy round bars obtained in different rolling processes, Arch. Metall. Mater. 60 (2015) 3001–3006, doi:10.1515/amm-2015-0479.
[27] P. Szota, S. Mróz, A. Stefanik, R. Mola, Analysis of the AZ31 magnesium alloy bars rolling process in modified stretching passes, Materwiss. Werksttech. 46 (2015) 285–293, doi:10.1002/mawe.201400349.
[28] J. Yu, H. Liao, J.H. Lee, Y.H. Moon, H.S. Yoon, J. Kim, T. Lee, Microstructural evolution of multi-pass caliber-rolled Mg–Sn and Mg–Sn–Mn alloys, Metals (Basel) 10 (2020) 1203, doi:10.3390/met10091203.
[29] A. Stefanik, P. Szota, S. Mroz, H. Dyja, Application of the three-high skew rolling to magnesium rods production, Mater. Test. 58 (2016) 438–441, doi:10.3139/120.110876.
[30] S. Dobatkin, S. Galkin, Y. Estrin, V. Serebryany, M. Diez, N. Martynenko, E. Lukyanova, V. Perezhogin, Grain refinement, texture, and mechanical properties of a magnesium alloy after radial-shear rolling, J. Alloys Compd. 774 (2019) 969–979, doi:10.1016/j.jallcom.2018.09.065.
[31] A. Stefanik, P. Szota, S. Mróz, Analysis of the Effect of Rolling Speed on the Capability to Produce Bimodal-Structure AZ31 Alloy Bars in the Three-High Skew Rolling Mill, Arch. Metall. Mater. (2020), doi:10.24425/amm.2020.131734.
[32] Z. Zhao, S.Y. Hong, Cooling strategies for cryogenic machining from a materials viewpoint, J. Mater. Eng. Perform. 1 (1992) 669–678, doi:10.1007/BF02649248.
[33] Y. Jiang, D. Chen, Z. Chen, J. Liu, Effect of cryogenic treatment on the microstructure and mechanical properties of AZ31 magnesium alloy, Mater. Manuf. Process. 25 (2010) 837–841, doi:10.1080/10426910903496862.
[34] H.L. Yu, C. Lu, A.K. Tieu, H.J. Li, A. Godbole, S.H. Zhang, Special rolling techniques for improvement of mechanical properties of ultrafine-grained metal sheets: a review, Adv. Eng. Mater. 18 (2016) 754–769, doi:10.1002/adem.201500369.
[35] V.S. Sarma, J. Wang, W.W. Jian, A. Kauffmann, H. Conrad, J. Freudenberger, Y.T. Zhu, Role of stacking fault energy in strengthening due to cryo-deformation of FCC metals, Mater. Sci. Eng. A. 527 (2010) 7624–7630, doi:10.1016/j.msea.2010.08.015.
[36] N.V. Ravi Kumar, J.J. Blandin, C. Desrayaud, F. Montheillet, M. Suéry, Grain refinement in AZ91 magnesium alloy during thermomechanical processing, Mater. Sci. Eng. A. 359 (2003) 150–157, doi:10.1016/S0921-5093(03)00334-4.
[37] H. Dieringa, Influence of cryogenic temperatures on the microstructure and mechanical properties of magnesium alloys: a review, Metals (Basel) 7 (2017), doi:10.3390/met7020038.
[38] J. Yong, C. Ding, J. Qiong, Effect of cryogenic thermocycling treatment on the structure and properties of magnesium alloy AZ91, Met. Sci. Heat Treat. 53 (2012) 589–591, doi:10.1007/s11041-012-9439-x.
[39] J. ru Luo, Y. qiong Yan, J. shan Zhang, L. zhong Zhuang, Microstructure and mechanical properties of cryorolled AZ31 magnesium alloy sheets with different initial textures, Int. J. Miner. Metall. Mater. 23 (2016) 827–834, doi:10.1007/s12613-016-1297-x.
[40] J. Luo, Y. Yan, J. Zhang, L. Zhuang, Microstructure and mechanical properties of a basal textured AZ31 magnesium alloy cryorolled at liquid-nitrogen temperature, Met. Mater. Int. 22 (2016) 637–641, doi:10.1007/s12540-016-5645-1.
[41] T. Murai, S.I. Matsuoka, S. Miyamoto, Y. Oki, Effects of extrusion conditions on microstructure and mechanical properties of AZ31B magnesium alloy extrusions, J. Mater. Process. Technol. 141 (2003) 207–212, doi:10.1016/S0924-0136(02)01106-8.
[42] Z.R. Zeng, Y.M. Zhu, R.L. Liu, S.W. Xu, C.H.J. Davies, J.F. Nie, N. Birbilis, Achieving exceptionally high strength in Mg–3Al–1Zn-0.3Mn extrusions via suppressing intergranular deformation, Acta Mater 160 (2018) 97–108, doi:10.1016/j.actamat.2018.08.045.
[43] S.H. Hsiang, J.L. Kuo, An investigation on the hot extrusion process of magnesium alloy sheet, J. Mater. Process. Technol. 140 (2003) 6–12, doi:10.1016/S0924-0136(03)00693-9.
[44] J. Bohlen, S.B. Yi, J. Swiostek, D. Letzig, H.G. Brokmeier, K.U. Kainer, Microstructure and texture development during hydrostatic extrusion of magnesium alloy AZ31, Scr. Mater. 53 (2005) 259–264, doi:10.1016/j.scriptamat.2005.03.036.

[45] Q. Yang, B. Jiang, H. Pan, B. Song, Z. Jiang, J. Dai, L. Wang, F. Pan, Influence of different extrusion processes on mechanical properties of magnesium alloy, J. Magnes. Alloy. 2 (2014) 220–224, doi:10.1016/j.jma.2014.10.001.
[46] Y. Li, L. Chen, J. Tang, G. Zhao, C. Zhang, Effects of asymmetric feeder on microstructure and mechanical properties of high strength Al-Zn-Mg alloy by hot extrusion, J. Alloys Compd. 749 (2018) 293–304, doi:10.1016/j.jallcom.2018.03.188.
[47] L.L. Chang, Y.N. Wang, X. Zhao, J.C. Huang, Microstructure and mechanical properties in an AZ31 magnesium alloy sheet fabricated by asymmetric hot extrusion, Mater. Sci. Eng. A. 496 (2008) 512–516, doi:10.1016/j.msea.2008.06.015.
[48] Y. Chen, Q. Wang, J. Peng, C. Zhai, W. Ding, Effects of extrusion ratio on the microstructure and mechanical properties of AZ31 Mg alloy, J. Mater. Process. Technol. 182 (2007) 281–285, doi:10.1016/j.jmatprotec.2006.08.012.
[49] S.J. Liang, Z.Y. Liu, E.D. Wang, Microstructure and mechanical properties of Mg-Al-Zn alloy sheet fabricated by cold extrusion, Mater. Lett. 62 (2008) 4009–4011, doi:10.1016/j.matlet.2008.05.045.
[50] W. Pachla, A. Mazur, J. Skiba, M. Kulczyk, S. Przybysz, Development of high-strength pure magnesium and wrought magnesium alloys AZ31, AZ61, and AZ91 processed by hydrostatic extrusion with back pressure, Int. J. Mater. Res. 103 (2012) 580–589, doi:10.3139/146.110721.
[51] Y. Huang, T.G. Langdon, Advances in ultrafine-grained materials, Mater. Today. 16 (2013) 85–93, doi:10.1016/j.mattod.2013.03.004.
[52] A. Yamashita, Z. Horita, T.G. Langdon, Improving the mechanical properties of magnesium and a magnesium alloy through severe plastic deformation, Mater. Sci. Eng. A. 300 (2001) 142–147, doi:10.1016/S0921-5093(00)01660-9.
[53] R.Z. Valiev, Y. Estrin, Z. Horita, T.G. Langdon, M.J. Zehetbauer, Y. Zhu, Producing bulk ultrafine-grained materials by severe plastic deformation: ten years Later, Jom 68 (2016) 1216–1226, doi:10.1007/s11837-016-1820-6.
[54] R.B. Figueiredo, T.G. Langdon, Principles of grain refinement and superplastic flow in magnesium alloys processed by ECAP, Mater. Sci. Eng. A. 501 (2009) 105–114, doi:10.1016/j.msea.2008.09.058.
[55] S.M. Fatemi, A. Zarei, M. Haghshenas, Accumulative roll bonding Of Az31 magnesium alloy, Int. J. Mod. Phys. B 22 (2008) 2833–2939, doi:10.1142/s0217979208047651.
[56] K. Nakashima, Z. Horita, M. Nemoto, T.G. Langdon, Influence of channel angle on the development of ultrafine grains in equal-channel angular pressing, Acta Mater 46 (1998) 1589–1599, doi:10.1016/S1359-6454(97)00355-8.
[57] M. Furukawa, Z. Horita, M. Nemoto, T.G. Langdon, Processing of metals by equal-channel angular pressing, J. Mater. Sci. 36 (2001) 2835–2843, doi:10.1023/A:1017932417043.
[58] M. Janeček, M. Popov, M.G. Krieger, R.J. Hellmig, Y. Estrin, Mechanical properties and microstructure of a Mg alloy AZ31 prepared by equal-channel angular pressing, Mater. Sci. Eng. A. 462 (2007) 116–120, doi:10.1016/j.msea.2006.01.174.
[59] M. Furukawa, Y. Iwahashi, Z. Horita, M. Nemoto, T.G. Langdon, The shearing characteristics associated with equal-channel angular pressing, Mater. Sci. Eng. A. 257 (1998) 328–332, doi:10.1016/S0921-5093(98)00750-3.
[60] M. Furukawa, Z. Horita, T.G. Langdon, Factors influencing the shearing patterns in equal-channel angular pressing, Mater. Sci. Eng. A. 332 (2002) 97–109, doi:10.1016/S0921-5093(01)01716-6.
[61] S.X. Ding, C.P. Chang, P.W. Kao, Effects of processing parameters on the grain refinement of magnesium alloy by equal-channel angular extrusion, Metall. Mater. Trans. A Phys. Metall. Mater. Sci. 40 (2009) 415–425, doi:10.1007/s11661-008-9747-3.
[62] K. Bryła, J. Dutkiewicz, L. Lityńska-dobrzyńska, L.L. Rokhlin, P. Kurtyka, Influence of number of ecap passes on microstructure and mechanical properties of az31 magnesium alloy, Arch. Metall. Mater. 57 (2012) 711–717, doi:10.2478/v10172-012-0077-5.
[63] S.J. Huang, C. Chiu, T.Y. Chou, E. Rabkin, Effect of equal channel angular pressing (ECAP) on hydrogen storage properties of commercial magnesium alloy AZ61, Int. J. Hydrogen Energy. 43 (2018) 4371–4380, doi:10.1016/j.ijhydene.2018.01.044.
[64] L. Jin, D. Lin, D. Mao, X. Zeng, B. Chen, W. Ding, Microstructure evolution of AZ31 Mg alloy during equal channel angular extrusion, Mater. Sci. Eng. A. 423 (2006) 247–252, doi:10.1016/j.msea.2006.02.045.
[65] A. Muralidhar, S. Narendranath, H. Shivananda Nayaka, Effect of equal channel angular pressing on AZ31 wrought magnesium alloys, J. Magnes. Alloy. 1 (2013) 336–340, doi:10.1016/j.jma.2013.11.007.
[66] A.G. Beer, M.R. Barnett, Microstructural development during hot working of Mg-3Al-1Zn, Metall. Mater. Trans. A Phys. Metall. Mater. Sci. 38 (2007) 1856–1867, doi:10.1007/s11661-007-9207-5.
[67] S. Wierzbinski, A. Korbel, J.J. Jonas, Structural and mechanical aspects of high temperature deformation of polycrystalline nickel, Mater. Sci. Technol. 8 (1992) 153–158 (United Kingdom), doi:10.1179/mst.1992.8.2.153.
[68] K. Xia, J.T. Wang, X. Wu, G. Chen, M. Gurvan, Equal channel angular pressing of magnesium alloy AZ31, Mater. Sci. Eng. A. (2005) 324–327 410-411, doi:10.1016/j.msea.2005.08.123.
[69] C. Xu, K. Xia, T.G. Langdon, Processing of a magnesium alloy by equal-channel angular pressing using a back-pressure, Mater. Sci. Eng. A. 527 (2009) 205–211, doi:10.1016/j.msea.2009.07.063.
[70] R.B. Figueiredo, T.G. Langdon, Developing superplasticity in a magnesium AZ31 alloy by ECAP, J. Mater. Sci. 43 (2008) 7366–7371, doi:10.1007/s10853-008-2846-0.
[71] H.K. Lin, J.C. Huang, T.G. Langdon, Relationship between texture and low temperature superplasticity in an extruded AZ31 Mg alloy processed by ECAP, Mater. Sci. Eng. A. 402 (2005) 250–257, doi:10.1016/j.msea.2005.04.018.
[72] R. Lapovok, Y. Estrin, M.V. Popov, T.G. Langdon, Enhanced superplasticity in a magnesium alloy processed by equal-channel angular pressing with a back-pressure, Adv. Eng. Mater. 10 (2008) 429–433, doi:10.1002/adem.200700363.
[73] R. Lapovok, Y. Estrin, M.V. Popov, S. Rundell, T. Williams, Enhanced superplasticity of magnesium alloy AZ31 obtained through equal-channel angular pressing with back-pressure, J. Mater. Sci. 43 (2008) 7372–7378, doi:10.1007/s10853-008-2685-z.
[74] F. Kang, J.Q. Liu, J.T. Wang, X. Zhao, The effect of hydrostatic pressure on the activation of non-basal slip in a magnesium alloy, Scr. Mater. 61 (2009) 844–847, doi:10.1016/j.scriptamat.2009.07.011.
[75] C.W. Su, L. Lu, M.O. Lai, Mechanical behaviour and texture of annealed AZ31 Mg alloy deformed by ECAP, Mater. Sci. Technol. 23 (2007) 290–296, doi:10.1179/174328407X161132.
[76] H.G. Svoboda, F. Vago, Superplastic behavior of AZ31 processed by ECAP, Procedia Mater. Sci. 9 (2015) 590–598, doi:10.1016/j.mspro.2015.05.034.
[77] C.F. Davis, A.J. Griebel, T.C. Lowe, Isothermal continuous equal channel angular pressing of magnesium alloy AZ31, Jom 72 (2020) 2603–2611, doi:10.1007/s11837-020-04195-4.
[78] M. Gzyl, A. Rosochowski, S. Boczkal, L. Olejnik, The role of microstructure and texture in controlling mechanical properties of AZ31B magnesium alloy processed by I-ECAP, Mater. Sci. Eng. A. 638 (2015) 20–29, doi:10.1016/j.msea.2015.04.055.
[79] A. Rosochowski, L. Olejnik, FEM simulation of incremental shear, AIP Conf. Proc. 907 (2007) 653–658. doi:10.1063/1.2729587.
[80] M. Gzyl, A. Rosochowski, R. Pesci, L. Olejnik, E. Yakushina, P. Wood, Mechanical properties and microstructure of az31b magnesium alloy processed by I-ECAP, Metall. Mater. Trans. A Phys. Metall. Mater. Sci. 45 (2014) 1609–1620, doi:10.1007/s11661-013-2094-z.
[81] A.P. Zhilyaev, G.V. Nurislamova, B.K. Kim, M.D. Baró, J.A. Szpunar, T.G. Langdon, Experimental parameters influencing grain refinement and microstructural evolution during high-pressure torsion, Acta Mater 51 (2003) 753–765, doi:10.1016/S1359-6454(02)00466-4.
[82] A.P. Zhilyaev, T.G. Langdon, Using high-pressure torsion for metal processing: fundamentals and applications, Prog. Mater. Sci. 53 (2008) 893–979, doi:10.1016/j.pmatsci.2008.03.002.
[83] K. Edalati, Z. Horita, A review on high-pressure torsion (HPT) from 1935 to 1988, Elsevier, 2016, doi:10.1016/j.msea.2015.11.074.

[84] M. Kawasaki, R.B. Figueiredo, T.G. Langdon, Twenty-five years of severe plastic deformation: recent developments in evaluating the degree of homogeneity through the thickness of disks processed by high-pressure torsion, J. Mater. Sci. 47 (2012) 7719–7725, doi:10.1007/s10853-012-6507-y.
[85] Y. Huang, R.B. Figueiredo, T. Baudin, A.L. Helbert, F. Brisset, T.G. Langdon, Microstructure and texture evolution in a magnesium alloy during processing by high-pressure torsion, Mater. Res. 16 (2013) 577–585, doi:10.1590/S1516-14392013005000025.
[86] Y. Huang, R.B. Figueiredo, T. Baudin, F. Brisset, T.G. Langdon, Evolution of strength and homogeneity in a magnesium AZ31 alloy processed by high-pressure torsion at different temperatures, Adv. Eng. Mater. 14 (2012) 1018–1026, doi:10.1002/adem.201200016.
[87] J. Stráská, M. Janeček, J. Gubicza, T. Krajňák, E.Y. Yoon, H.S. Kim, Evolution of microstructure and hardness in AZ31 alloy processed by high pressure torsion, Mater. Sci. Eng. A. 625 (2015) 98–106, doi:10.1016/j.msea.2014.12.005.
[88] J. Vrátná, M. Janeček, J. Čížek, D.J. Lee, E.Y. Yoon, H.S. Kim, Mechanical properties and microstructure evolution in ultrafine-grained AZ31 alloy processed by severe plastic deformation, J. Mater. Sci. 48 (2013) 4705–4712, doi:10.1007/s10853-013-7151-x.
[89] T. Masuda, Z. Horita, Grain refinement of AZ31 and AZ61 Mg alloys through room temperature processing by up-scaled high-pressure torsion, Mater. Trans. 60 (2019) 1104–1110, doi:10.2320/matertrans.M2018308.
[90] R.B. Figueiredo, T.G. Langdon, Development of structural heterogeneities in a magnesium alloy processed by high-pressure torsion, Mater. Sci. Eng. A. 528 (2011) 4500–4506, doi:10.1016/j.msea.2011.02.048.
[91] R.B. Figueiredo, T.G. Langdon, Processing magnesium and its alloys by high-pressure torsion: an overview, Adv. Eng. Mater. 21 (2019) 1–15, doi:10.1002/adem.201801039.
[92] J. Xu, X. Wang, M. Shirooyeh, G. Xing, D. Shan, B. Guo, T.G. Langdon, Microhardness, microstructure and tensile behavior of an AZ31 magnesium alloy processed by high-pressure torsion, J. Mater. Sci. 50 (2015) 7424–7436, doi:10.1007/s10853-015-9300-x.
[93] R.B. Figueiredo, P.H.R. Pereira, T.G. Langdon, Low temperature superplasticity in ultrafine-grained AZ31 alloy, Defect Diffus. Forum. 385 DDF (2018) 59–64, doi:10.4028/www.scientific.net/DDF.385.59.
[94] L.R.C. Malheiros, R.B. Figueiredo, T.G. Langdon, Grain size and microhardness evolution during annealing of a magnesium alloy processed by high-pressure torsion, J. Mater. Res. Technol. 4 (2015) 14–17, doi:10.1016/j.jmrt.2014.10.008.
[95] R.B. Figueiredo, T.G. Langdon, Using high-pressure torsion to achieve superplasticity in an az91 magnesium alloy, Metals (Basel). 10 (2020) 1–10. doi:10.3390/met10050681.
[96] P. Serre, R.B. Figueiredo, N. Gao, T.G. Langdon, Influence of strain rate on the characteristics of a magnesium alloy processed by high-pressure torsion, Mater. Sci. Eng. A. 528 (2011) 3601–3608, doi:10.1016/j.msea.2011.01.066.
[97] S.M. Ghalehbandi, M. Malaki, applied sciences Accumulative Roll Bonding — A Review, 2019.
[98] F. Schwarz, K. Lange, L. Krüger, R. Kawalla, S. Reichelt, Microstructural and mechanical characterization of ARB AZ31, Mater. Sci. Forum. 765 (2013) 403–407, doi:10.4028/www.scientific.net/MSF.765.403.
[99] Z. Trojanová, J. Džugan, K. Halmešová, G. Németh, P. Minárik, P. Lukáč, J. Bohlen, Influence of accumulative roll bonding on the texture and tensile properties of an AZ31 magnesium alloy sheets, Materials (Basel) 11 (2018), doi:10.3390/ma11010073.
[100] A.A. Roostaei, A. Zarei-Hanzaki, H.R. Abedi, M.R. Rokni, An investigation into the mechanical behavior and microstructural evolution of the accumulative roll bonded AZ31 Mg alloy upon annealing, Mater. Des. 32 (2011) 2963–2968, doi:10.1016/j.matdes.2011.01.038.
[101] Q.F. WANG, X.P. XIAO, J. HU, W.W. XU, X.Q. ZHAO, S.J. ZHAO, An Ultrafine-Grained AZ31 Magnesium Alloy Sheet With Enhanced Superplasticity Prepared by Accumulative Roll Bonding, J. Iron Steel Res. Int. 14 (2007) 167–172, doi:10.1016/S1006-706X(08)60073-4.
[102] M.T. Pérez-Prado, J.A. Del Valle, O.A. Ruano, Grain refinement of MG-Al-Zn alloys via accumulative roll bonding, Scr. Mater. 51 (2004) 1093–1097, doi:10.1016/j.scriptamat.2004.07.028.
[103] H.K. Lin, J.C. Huang, High strain rate and/or low temperature superplasticity in AZ31 Mg alloys processed by simple high-ratio extrusion methods, Mater. Trans. 43 (2002) 2424–2432, doi:10.2320/matertrans.43.2424.
[104] M.Y. Zhan, W.W. Zhang, D.T. Zhang, Production of Mg-Al-Zn magnesium alloy sheets with ultrafine-grain microstructure by accumulative roll-bonding, Trans. Nonferrous Met. Soc. China (English Ed.) 21 (2011) 991–997 10.1016/S1003-6326(11)60811-X.
[105] C.S. Hsu, Q. Li, Processing and characterization of Ti64/AZ31 multilayered structure by roll bonding, Conf. Proc. Soc. Exp. Mech. Ser. 9 (2018) 73–78, doi:10.1007/978-3-319-62834-9_10.
[106] X. Luo, T. Huang, Y. Wang, Y. Xin, G. Wu, Strong and ductile AZ31 Mg alloy with a layered bimodal structure, Sci. Rep. 9 (2019) 2–10, doi:10.1038/s41598-019-41987-4.
[107] P. Kumar, A. Madhup, P.R. Kalvala, S. Suwas, Texture evaluation in AZ31/AZ31 multilayer and AZ31/AA5068 laminar composite during accumulative roll bonding, Def. Technol. 16 (2020) 514–519, doi:10.1016/j.dt.2019.08.014.
[108] M.Y. Zhan, Y.Y. Li, W.P. Chen, W.D. Chen, Microstructure and mechanical properties of Mg-Al-Zn alloy sheets severely deformed by accumulative roll-bonding, J. Mater. Sci. 42 (2007) 9256–9261, doi:10.1007/s10853-007-1885-2.
[109] H.S. Liu, B. Zhang, G.P. Zhang, Microstructures and Mechanical Properties of Al/Mg Alloy Multilayered Composites Produced by Accumulative Roll Bonding, J. Mater. Sci. Technol. 27 (2011) 15–21, doi:10.1016/S1005-0302(11)60019-4.
[110] Z.M. Liu, H.M. Chen, W.P. Guo, J. Zhang, Y.X. Jin, Interface and damping capacity of Mg/Al multilayered composite produced by accumulative roll bonding, Mater. Sci. Forum. 849 (2016) 838–843, doi:10.4028/www.scientific.net/MSF.849.838.
[111] R. Abedi, A. Akbarzadeh, Bond strength and mechanical properties of three-layered St/AZ31/St composite fabricated by roll bonding, Mater. Des. 88 (2015) 880–888, doi:10.1016/j.matdes.2015.09.043.
[112] M. Abbasi, S.A. Sajjadi, Mechanical properties and interface evaluation of Al/AZ31 multilayer composites produced by ARB at different rolling temperatures, J. Mater. Eng. Perform. 27 (2018) 3508–3520, doi:10.1007/s11665-018-3423-6.
[113] Z. Lv, X. Ren, W. Wang, X. Gao, W. Li, Microstructure and Mechanical Properties of Mg/2wt.%SiCp Nanocomposite Fabricated by ARB Process, J. Nanomater. (2016) 2016, doi:10.1155/2016/6034790.
[114] A. Sadeghi, A. Akbarzadeh, Development of nanostructure in AZ31 magnesium alloy during accumulative roll bonding process, Int. J. Nanomanuf. 5 (2010) 225–231, doi:10.1504/IJNM.2010.033864.
[115] S. Rachakonda, S.N. Dwivedi, Application of the finite element method in metal forming process design, CAD/CAM Robot. Factories Futur. ’90. (1991) 253–258. doi:10.1007/978-3-642-85838-3_35.
[116] Z. Jiang, H. Xie, Application of finite element analysis in multiscale metal forming process, finite element method - simulation, numerical analysis and solution techniques, Răzvan Păcurar, IntechOpen (2017), doi:10.5772/intechopen.71880.
[117] P. Groover Mikell, Fundamentals of Modern Manufacturing: Materials, Processes, and Systems, 7th Edition, J. Wiley & Sons, Hoboken, NJ, 2007 ISBN: 978-1-119-47521-7.
[118] Q. Jin, W. Wang, R. Jiang, L.N.S. Chiu, D. Liu, W. Yan, A numerical study on contact condition and wear of roller in cold rolling, Metals (Basel) 7 (2017), doi:10.3390/met7090376.
[119] M. Pekguleryuz, N.R. Neelameggham, R.S. Beals, E.A. Nyberg, Magnesium technology, Magnes. Technol. (2008).
[120] A. Murillo-Marrodán, E. García, F. Cortés, Friction modelling of a hot rolling process by means of the finite element method, Lect. Notes Eng. Comput. Sci. 2230 (2017) 965–969.
[121] D. Liu, Z. Liu, L. Wang, Simulation of rolling process of AZ31 magnesium alloy sheet, Procedia Eng 81 (2014) 173–178, doi:10.1016/j.proeng.2014.09.146.

[122] H. Hu, Z. Zhai, H. Wang, J.Z. Fan, Extrusion-shear of AZ31 alloy billets with low temperature and high speed by using three-dimensional finite element modeling and experiments, Mater. Res. 17 (2014) 987–995, doi:10.1590/1516-1439.260914.
[123] P. Li, S.R. Wang, Y. Wang, G.J. Xue, The extrusion behavior of AZ31 mg alloys by finite element simulation, Adv. Mater. Res. 906 (2014) 285–288, doi:10.4028/www.scientific.net/amr.906.285.
[124] T. Walde, H. Riedel, Modeling texture evolution during hot rolling of magnesium alloy AZ31, Mater. Sci. Eng. A. 443 (2007) 277–284, doi:10.1016/j.msea.2006.09.028.
[125] R.A. Lebensohn, C.N. Tomé, A self-consistent anisotropic approach for the simulation of plastic deformation and texture development of polycrystals: application to zirconium alloys, Acta Metall. Mater. 41 (1993) 2611–2624 doi:10.1016/0956-7151(93)90130-K.
[126] S.R. Kalidindi, Incorporation of deformation twinning in models, Int. J. Plast. 46 (1998) 267–290.
[127] M. Chen, W. Yuan, H. Li, Z. Zou, Modeling and simulation of dynamic recrystallization behaviors of magnesium alloy AZ31B using cellular automaton method, Comput. Mater. Sci. 136 (2017) 163–172, doi:10.1016/j.commatsci.2017.05.009.
[128] G. Faraji, H.S. Kim, H.T. Kashi, Severe Plastic Deformation Methods for Bulk Samples, 2018. doi:10.1016/b978-0-12-813518-1.00002-3.
[129] T.C. Lowe, R.Z. Valiev, The use of severe plastic deformation techniques in grain refinement, JOM 56 (2004) 64–68, doi:10.1007/s11837-004-0295-z.
[130] G. Ren, G. Zhao, S. Xu, Numerical simulation and experimental study of AZ31 magnesium alloy deformation behavior in ECAP, Adv. Mater. Res. (2011) 227–231 148-149, doi:10.4028/www.scientific.net/AMR.148-149.227.
[131] Y. Xia, B. Peng, C. Zhou, R. Pan, S. Chen, Effect of deformation homogeneity on grain refinement of AZ31 magnesium alloys based on FEA during ECAP, Mater. Sci. Forum. 850 (2016) 281–286, doi:10.4028/www.scientific.net/MSF.850.281.
[132] H. jun HU, D. fei ZHANG, F. sheng PAN, Die structure optimization of equal channel angular extrusion for AZ31 magnesium alloy based on finite element method, Trans. Nonferrous Met. Soc. China (English Ed. 20 (2010) 259–266, doi:10.1016/S1003-6326(09)60132-1.
[133] Y. Xia, B. Peng, C. Zhou, R. Pan, S. Chen, Effect of deformation homogeneity on grain refinement of AZ31 magnesium alloys based on FEA during ECAP, Mater. Sci. Forum. 850 (2016) 281–286, doi:10.4028/www.scientific.net/MSF.850.281.
[134] W. Wei, W. Zhang, K.X. Wei, Y. Zhong, G. Cheng, J. Hu, Finite element analysis of deformation behavior in continuous ECAP process, Mater. Sci. Eng. A. 516 (2009) 111–118, doi:10.1016/j.msea.2009.03.001.
[135] S. Xu, C. Jing, G. Ren, P. Liu, Finite element simulation of die design for warm equal channel angular extrusion process of AZ31 alloy and its experimental investigation, Mater. Sci. Forum. (2011) 75–79 667-669, doi:10.4028/www.scientific.net/MSF.667-669.75.
[136] Z. Xie, J. Xie, Y. Hong, X. Wu, Influence of processing temperature on microstructure and microhardness of copper subjected to high-pressure torsion, Sci. China Technol. Sci. 53 (2010) 1534–1539, doi:10.1007/s11431-010-3157-7.
[137] Y. Song, W. Wang, D. Gao, E.Y. Yoon, D.J. Lee, H.S. Kim, Finite element analysis of the effect of friction in high pressure torsion, Met. Mater. Int. 20 (2014) 445–450, doi:10.1007/s12540-014-3007-4.
[138] P.H.R. Pereira, R.B. Figueiredo, P.R. Cetlin, T.G. Langdon, Using finite element modelling to examine the flow process and temperature evolution in HPT under different constraining conditions, IOP Conf. Ser. Mater. Sci. Eng. 63 (2014), doi:10.1088/1757-899X/63/1/012041.
[139] R.B. Figueiredo, P.R. Cetlin, T.G. Langdon, Using finite element modeling to examine the flow processes in quasi-constrained high-pressure torsion, Mater. Sci. Eng. A. 528 (2011) 8198–8204, doi:10.1016/j.msea.2011.07.040.
[140] R.B. Figueiredo, M.T.P. Aguilar, P.R. Cetlin, T.G. Langdon, Analysis of plastic flow during high-pressure torsion, J. Mater. Sci. 47 (2012) 7807–7814, doi:10.1007/s10853-012-6506-z.
[141] A.A. Roostaei, A. Zarei-Hanzaki, M.H. Parsa, S.M. Fatemi-Varzaneh, An analysis to plastic deformation behavior of AZ31 alloys during accumulative roll bonding process, J. Mater. Sci. 45 (2010) 4494–4500, doi:10.1007/s10853-010-4540-2.
[142] T. Inoue, A. Yanagida, J. Yanagimoto, Finite element simulation of accumulative roll-bonding process, Mater. Lett. 106 (2013) 37–40, doi:10.1016/j.matlet.2013.04.093.
[143] H. Wang, L. Su, H. Yu, C. Lu, A.K. Tieu, Y. Liu, J. Zhang, A new finite element model for multi-cycle accumulative roll-bonding process and experiment verification, Mater. Sci. Eng. A. 726 (2018) 93–101, doi:10.1016/j.msea.2018.04.040.
[144] S.M. Arab, A. Akbarzadeh, On the cold rolling of AZ31 Mg alloy after equal channel angular pressing, J. Magnes. Alloy. 2 (2014) 203–207, doi:10.1016/j.jma.2014.08.003.
[145] P. Lukáč, R. Kocich, M. Greger, O. Padalka, Z. Száraz, Microstructure of AZ31 and AZ61 Mg alloys prepared by rolling and ECAP, Kov. Mater. 45 (2007) 115–120.
[146] W.J. Kim, Y.K. Sa, Micro-extrusion of ECAP processed magnesium alloy for production of high strength magnesium micro-gears, Scr. Mater. 54 (2006) 1391–1395, doi:10.1016/j.scriptamat.2005.11.066.
[147] C. Huang, X. Jia, Z. Zhang, Modeling and simulation of the static recrystallization of 5754 aluminium alloy by cellular automaton, Metals 8 (2018) 585.